A new quotidian equation of state (QEOS) for hot dense matter

R. M. More, K. H. Warren, D. A. Young, and G. B. Zimmerman
Lawrence Livermore National Laboratory, University of California, Livermore, California 94550

The quotidian equation of state (QEOS) is a general-purpose equation of state model for use in hydrodynamic simulation of high-pressure phenomena. Electronic properties are obtained from a modified Thomas–Fermi statistical model, while ion thermal motion is described by a multiphase equation of state combining Debye, Grüneisen, Lindemann, and fluid-scaling laws. The theory gives smooth and usable predictions for ionization state, pressure, energy, entropy, and Helmholtz free energy. When necessary, the results may be modified by a temperature-dependent pressure multiplier which greatly extends the class of materials that can be treated with reasonable accuracy. In this paper a comprehensive evaluation of the resulting thermodynamic data is given including comparison with other theories and shock-wave data.

I. INTRODUCTION

Many contemporary research programs investigate consequences of high energy concentration in a solid or dense vapor target. Temperatures above 1 eV $\simeq 11\,600$ K will be produced when the energy exceeds $\sim 10^4$ J/g. Such conditions are achieved in laser-produced plasmas, laser fusion, exploding wires, magnetically or electrically driven foils, self-pinching discharges, high-velocity impacts including meteorite impacts and gun experiments, and in targets heated by ion or electron beams.[1]

Experiments at high energy–density are often analyzed by numerical hydrodynamic simulations which calculate space- and time-dependent density–temperature profiles, $\rho(r,t)$ and $T(r,t)$. An essential input to the simulations is a knowledge of the material equation of state (EOS) which usually takes the form of pressure p and energy E as functions of ρ and T. The success of an experimental program may depend on the availability and quality of this EOS data.

For typical applications, one desires EOS data having an accuracy of 15%–20% or better. Hydrodynamic codes encounter numerical difficulties unless the data is represented by smooth functions of density and temperature; they also require that the specific heat $(\partial E/\partial T)_\rho$ and sound speed $[(\partial p/\partial \rho)_s]^{1/2}$ be positive at the conditions of interest. Pressure and energy should be thermodynamically consistent [see Eq. (6) below]. Of course the data must be obtained in a timely manner in order to be useful.

We have developed an approximate method for constructing equation of state information which appears to meet most of these requirements. The electron ionization-equilibrium EOS is taken from the Thomas–Fermi statistical model of Feynman, Metropolis, and Teller,[2] supplemented by a semiempirical bonding correction in a form proposed by Barnes.[3] The ion equation of state combines Debye, Grüneisen, and liquid scaling-law theories and is based on unpublished work of Cowan.[4]

In this paper we present the theory in detail, add new features that greatly extend the versatility of the method, describe the computational implementation, and give a detailed and critical evaluation of the resulting thermodynamic data with many examples.

A. Overview of QEOS

For purposes of orientation we begin with an example: Figure 1 shows contours of constant entropy calculated by a quotidian equation of state (QEOS) for aluminum plasmas and the predicted liquid–vapor phase boundary together with the *principal Hugoniot* locus, the set of states produced by shock compression starting from the cold solid state. These adiabatic contours are smooth and well behaved; their accuracy is discussed in Sec. VIII.

Our main interest in this paper is the physical basis for the equations used by QEOS and the comparison with experimental data. However, it may assist the reader if we summarize the main features of QEOS as seen by a hypothetical hydrodynamic code user.

(1) QEOS is a self-contained theoretical model that requires no external data base. The inputs are simply the material composition and properties of the cold solid (its density and bulk modulus or sound speed). If the resulting equation of state is not satisfactory, one can increase its accuracy by adjusting various parameters.

(2) The outputs include pressure, energy, entropy, Helmholtz free energy, and derivatives (e.g., $\partial p/\partial \rho$, $\partial p/\partial T$, etc.). The entropy data enable us to measure and compare the importance of heat flow, shocks, or other nonadiabatic processes, a powerful tool for detailed analysis of nonideal hydrodynamic flows.

(3) Because QEOS supplies the complete set of thermodynamic properties including entropy, it becomes possible to supplement it with temperature-dependent pressure multipliers that greatly increase the flexibility in practical applications (see Sec. VI).

(4) The calculated pressure and energy exactly satisfy the condition of thermodynamic consistency and we have developed a new table interpolation method that preserves this consistency (Sec. IV). The results are smooth functions of ρ and T and are remarkably free of numerical noise.

(5) Electron and ion pressure and energy are calculated separately; this is important for plasmas in which the two species have unequal temperatures. (See Sec. III.)

(6) The computer code containing the QEOS theory is sufficiently fast and reliable to be used as a subroutine of
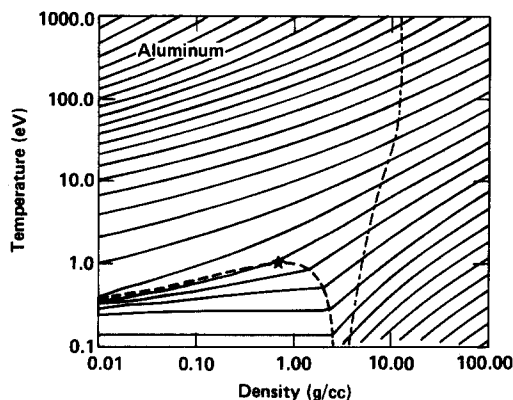
FIG. 1. Aluminum equation of state produced by QEOS. The contours are curves of constant total entropy. The QEOS critical point is shown as a star on a dashed curve which outlines the liquid–vapor two-phase region. The dot–dash curve is the principal Hugoniot beginning from the cold solid. The QEOS results are evidently smooth and usable, even if not perfectly correct, throughout the temperature range shown (see Sec. VIII).

hydrodynamic codes such as LASNEX.[5] The computational applications are discussed in Sec. IX.

(7) QEOS is the product of a long evolution[6] and has been tested against a large number of experiments of different types. While it is not suited to all materials, we are able to identify cases where the largest errors or uncertainties exist (see Sec. VIII). For many practical applications, QEOS is entirely adequate.

With all these advantages it is no surprise that there are also some difficulties. These include a limitation to equilibrium ionization states [the charge state Q corresponds to local thermodynamic equilibrium (LTE) at the electron temperature T_e], neglect of (small) quantum shell effects in ionization, neglect of solid–solid crystal phase transitions, inaccuracy of the liquid–vapor critical point for many materials, and a rather inaccurate treatment of polyatomic molecular materials. These defects (and others) are examined in the following sections.

Despite the defects, QEOS provides a very robust description of matter at sufficiently high energy density. Probably any future effort to develop a comprehensive thermodynamic model will benefit from careful examination of the choices made in defining QEOS.

This paper is a companion, both in scope and methods, to a recent general-purpose theory of electron conduction coefficients of hot dense matter.[7] As in that work, the goal is to develop a simple theory that gives reasonable predictions for a broad range of materials, densities, and temperatures (see Sec. IX).

B. Effects of nonideal EOS

One can illustrate typical nonideal effects in the hydrodynamics of hot dense plasmas by comparing calculations of flow with ideal gas and nonideal ("real") equations of state.[8] This comparison shows the importance of nonideal phenomena.

We consider the adiabatic expansion of an aluminum

foil initially at a uniform density $\rho_0 = 0.1$ g/cm^3 and temperature $T_0 = 50$ eV. This foil is assumed to be 1 cm thick and assumed to have sufficiently large area that it expands in a planar (one-dimensional) flow.

At early times the expansion consists of two independent rarefactions which move from the left and right surfaces toward the center of the foil with the sound speed c_0 of the initial state ρ_0, T_0.

The ideal gas flow is given in closed form by a well-known Riemann solution[9] of the hydrodynamic equations

$$\rho(x,t) = \begin{cases} 0, & x > 3c_0 t, \\ \rho_0(\tfrac{3}{4} - x/4c_0 t)^3, & 3c_0 t > x > (-c_0 t), \\ \rho_0, & (-c_0 t) > x, \end{cases} \quad (1)$$

$$v(x,t) = \begin{cases} \tfrac{3}{4}(c_0 + x/t), & 3c_0 t > x > (-c_0 t), \\ 0, & (-c_0 t) > x. \end{cases}$$

The temperature $T(x,t)$ is given by the ideal gas adiabatic relation, $T/T_0 = (\rho/\rho_0)^{2/3}$. In Eq. (1) the coordinate x is measured from the initial right-hand surface of the foil; of course the left surface expands also. The equations apply only for a limited time interval $t < L/2c_0$, where $L = 1$ cm is the foil thickness; after this time the rarefactions interact and the analytic solution becomes invalid.

Figures 2(a) and 2(b) compare this ideal gas flow with
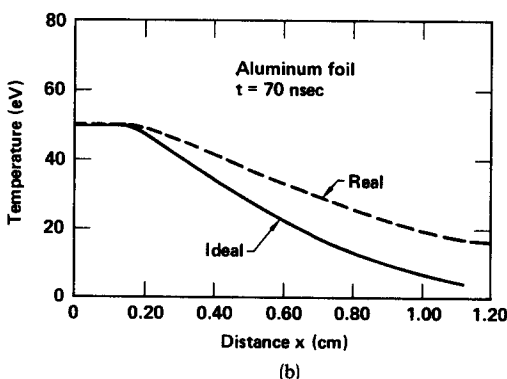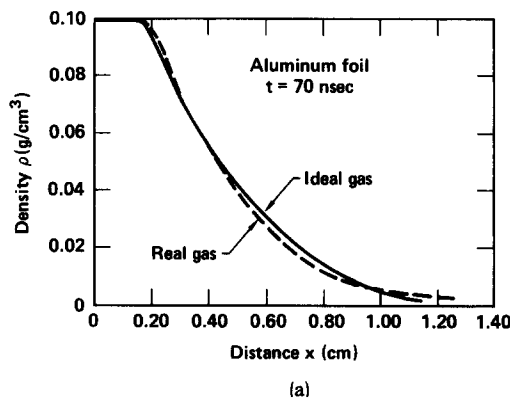

(a)

(b)

FIG. 2. Hydrodynamic modeling with aluminum. (a) Densities in the hydrodynamic flow of an aluminum foil which begins expanding at $t = 0$ from $\rho_0 = 0.1$ g/cm^3 and $T_0 = 50$ eV. The original position of the foil surface is $x = 0.5$ cm. Calculations with real and ideal EOS models are quite similar. (b) Temperatures for the flow problem of Fig. 2(a). The temperatures differ by as much as a factor of 4; this difference occurs because the real equation of state includes the large energy released by recombination in the expanding plasma.

numerically calculated results based on a realistic theoretical equation of state. In the figures, the coordinate x is measured from the center of the foil.

Comparing real and ideal flows, one sees the density profiles are very similar, but the temperature profiles are not. Outer layers of the "real" problem have a temperature *as much as four times higher* than the ideal flow.

This substantial difference results mainly from energy released by recombination in the expanding foil. Each electron which recombines releases $\sim 5kT$ to the remaining free electrons. Obviously this energy release is very important to the plasma dynamics; in general, ionization/recombination energy is one of the main ingredients of a realistic equation of state. In QEOS this energy is obtained from the Thomas–Fermi (TF) theory.

The comparison shown in Figs. 2(a) and 2(b) does not attempt to illustrate the complexities of real equations of state, which are more pronounced at other density-temperature conditions. In this case, several other theories (e.g., Saha equation) would give results very much like QEOS. The example clearly shows, however, the inadequacy of an ideal gas model that neglects recombination and ionization phenomena.

C. Equation of state models

The literature of dense plasma equation of state research is very extensive and we only cite a few review articles here. The interested reader will have no difficulty using these sources to develop an extensive bibliography.

The general physics of matter at high energy density is reviewed in books by Caldirola and Knoepfel[1] or Zel'dovich and Raizer.[9] Ross[10] reviews recent research on thermodynamic properties in the pressure range below 10 Mbar, with special emphasis on phenomenological models for shock-wave data. Other useful specialized reviews are given by Brush,[11] Kirzhnitz *et al.*,[12] More,[13] Alekseev *et al.*,[14] Bushman and Fortov,[15] and Godwal *et al.*[16]

A very useful compilation of high-pressure shock-wave data has been prepared by Marsh.[17]

Tabular equation of state data is collected at several national laboratories; the SESAME collection sees especially widespread application.[18] In many respects QEOS is an outgrowth of the original SESAME model,[6] but while QEOS represents a definite set of approximate equations, SESAME has become a file structure capable of accepting EOS data from any source.

The most significant differences between QEOS and the library systems are discussed in Sec. IX; in general terms, hydrodynamic code users will find QEOS data to be smoother, more flexible, and to have superior numerical quality, while for some materials the library data may be more accurate at certain density–temperature conditions.

II. EOS STRUCTURE

QEOS adopts the usual assumption[9,13] that electron and ion quantities are additive to sufficient accuracy. A more rigorous description is possible but would require substantial alteration of the usual hydrodynamic equations.[19,20] (See Sec. III for further discussion of this point.)

With the additive assumption, the Helmholtz free energy per gram is

$$F(\rho, T_e, T_i) = F_i(\rho, T_i) + F_e(\rho, T_e) + F_b(\rho, T_e). \quad (2)$$

In Eq. (2), F_i is the ion free energy calculated from formulas (Sec. III) which reduce to the ion ideal gas at high temperature ($T \gg T_{\text{melt}}$) and to a Debye–Grüneisen law in the solid phase ($T < T_{\text{melt}}$). Also, F_e is the semiclassical electron free energy obtained from the spherical-cell Thomas–Fermi theory, including ionization and core-repulsion effects (Sec. IV). In addition, F_b is a semiempirical correction for chemical bonding effects in the solid state; F_b can also represent exchange or other quantum effects (Sec. V).

In order to see how the theory works it is important to understand which terms make the largest contributions, but this depends on composition, density, and temperature.

For materials with large atomic number (e.g., $Z > 10$) at temperatures above $\simeq 10$ eV, most of the pressure comes from free electrons and the key variable is the ionization state. The Thomas–Fermi ionization model gives a reasonably accurate representation of these electron contributions, omitting small effects ($\leqslant 15\%$) associated with quantum shell structure in the ionization potentials (Sec. IV). At very high densities the free electrons are degenerate and produce a large pressure independent of temperature; this effect is also reproduced by the Thomas–Fermi theory.

The largest inaccuracy in the Thomas–Fermi pressure occurs near the cold solid ($\rho = \rho_s$, $T \cong 0$); in this case the TF theory may predict a multimegabar pressure where the actual pressure is zero. In QEOS this discrepancy is corrected with the empirical bonding correction F_b, which has little effect away from the region near $\rho = \rho_s$, $T \cong 0$ (see Sec. V).

Ions make a large contribution to pressure for low temperatures (e.g., $T < 10$ eV) and low densities where one has a neutral atomic gas, and also near the solid density. At higher density ($\rho \geqslant 2\rho_s$) and/or higher temperatures, the ion pressure is usually much less than the electron pressure. For low-Z materials such as hydrogen, the ions make a significant contribution at any density and temperature.

The pressure p, entropy S, and energy E are obtained from the free energy of Eq. (2) according to the following equations:

$$p_e = \rho^2 \frac{\partial F_e}{\partial \rho}, \quad S_e = -\frac{\partial F_e}{\partial T_e}, \quad E_e = F_e + T_e S_e, \quad (3)$$

$$p_b = \rho^2 \frac{\partial F_b}{\partial \rho}, \quad S_b = -\frac{\partial F_b}{\partial T_e}, \quad E_b = F_b + T_e S_b, \quad (4)$$

$$p_i = \rho^2 \frac{\partial F_i}{\partial \rho}, \quad S_i = -\frac{\partial F_i}{\partial T_i}, \quad E_i = F_i = T_i S_i. \quad (5)$$

Here F and E are energies per gram and ρ is the mass density (g/cm^3). The total pressure, entropy, and energy are sums of the additive contributions shown. The complete EOS is thermodynamically consistent because each part is; for example,

$$\rho^2 \left(\frac{\partial E_e}{\partial \rho} \right) = p_e - T_e \left(\frac{\partial p_e}{\partial T_e} \right). \quad (6)$$

In Sec. IV we describe a tabular representation of the Thomas–Fermi free energy F_e which exactly satisfies this equa-

3061   Phys. Fluids, Vol. 31, No. 10, October 1988

More *et al.*   3061

tion. Bonding and ion free energies come from analytic formulas which automatically obey the consistency condition. The bonding correction F_b is independent of temperature, so that $S_b = 0$, $E_b = F_b$, and $p_b = \rho^2\, \partial E_b/\partial\rho$.

QEOS was originally devised for application to laser fusion target calculations, where the temperature reaches 0.1–1 keV.[4–6] However, even these fusion plasma calculations begin with irradiation of cold condensed matter and the initial time has a strong influence on the subsequent implosion dynamics. The cold solid must therefore be handled with reasonable accuracy. In practice we require (1) zero total pressure at the correct normal density ρ_s,

$$p(\rho_s, 0) = 0; \qquad (7)$$

(2) approximately correct density jumps for shock waves starting from the cold solid (i.e., a correct shock speed); and (3) smooth variation of pressure and energy between the cold solid and the high-pressure plasma state.

These goals are achieved by careful choice of the functional dependence on ρ and T and by explicit introduction of the known solid density ρ_s and solid-state sound speed c_s (or equivalently, bulk modulus B), which determine the parameters of the semiempirical bonding correction F_b.

III. ION EQUATION OF STATE

The ion equation of state describes the pressure and energy associated with ion or nuclear motion. In QEOS these ion properties are completely independent of the electrons, except for the constraint that the charge densities be equal. In particular, the ion thermodynamic variables are assumed to be independent of the electron temperature.

This is a very strong assumption which cannot be correct in all cases. For fully ionized ideal gas conditions, there is no difficulty. At higher densities or lower temperatures, the Coulomb potential $U(R) = Q^2 e^2/R$ between ions becomes important, but U depends upon the electron temperature through the ion charge state $Q(T_e)$, and it is impossible to justify an approximation which neglects this dependence.

In practice this difficulty is alleviated by two facts: first, electron and ion temperatures are often nearly equal in the dense plasmas; and second, for materials with charge states Q greater than 10, the total ion contribution to the EOS is not large ($\leqslant 10\%$). In this circumstance one probably obtains an adequate hydrodynamic EOS from the additive EOS model.

If one wants to be confident of a theoretical calculation of the ion temperature, then a more rigorous theoretical treatment would be required. Such a theory is outlined in a series of recent papers.[8,13,19–21]

In this section we examine the calculation of ion thermodynamic properties assuming the ion motion to be separable from the electronic state. Our main interest is in the low temperature conditions ($T \leqslant 10$ eV) where ions make a significant contribution to the total equation of state.

A. Well-known laws

Ion thermodynamic properties are governed by known general laws in several limiting cases (Fig. 3). By incorporating all these special cases, QEOS obtains a robust ability to
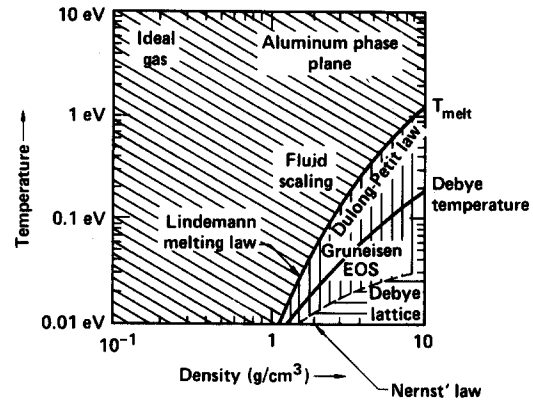

FIG. 3. Schematic illustration of the components of the ion equation of state.

imitate the behavior of real materials at most density-temperature conditions.

Throughout this section, T is the ion temperature and k is the Boltzmann constant; however, we often will express T in electron volts (eV) and then omit the Boltzmann constant.

(1) The *ideal gas law* applies at either very high temperature or very low density:

$$p_i = \rho k T/AM_p,$$
$$E_i = \tfrac{3}{2} kT/AM_p, \qquad (8)$$
$$S_i = (k/AM_p)\left[S_0 + \tfrac{3}{2}\log(kT/\rho^{2/3})\right].$$

These formulas give pressure, energy, and entropy associated with ion (nuclear) coordinates. The dimensionless entropy constant S_0 is determined by the *Sackur–Tetrode equation*,[22]

$$S_0 = \tfrac{5}{2} + \log(g\, AM_p) - \tfrac{3}{2}\log(h^2/2\pi\, AM_p), \qquad (9a)$$

where $g = (2I + 1)$ is the nuclear spin degeneracy, A is the atomic weight, and M_p is the atomic mass unit (1.66×10^{-24} g). With ρ and T given in g/cm³ and eV, the dimensionless ideal gas entropy constant S_0 becomes

$$S_0 = 8.4662 + \log(g\, A^{5/2}). \qquad (9b)$$

(2) The *fluid scaling law*. For nonideal dense fluids, several approaches[23,24,25] indicate that corrections to the ideal gas law scale with the ratio T_m/T, where $T_m = T_m(\rho)$ is the density-dependent melting temperature. In QEOS, this scaling law is written

$$E_i = \frac{3}{2}\frac{kT}{AM_p}\left[1 + f\!\left(\frac{T_m}{T}\right)\right], \qquad (10a)$$

$$p_i = \frac{\rho kT}{AM_p}\left[1 + \gamma_F(\rho)f\!\left(\frac{T_m}{T}\right)\right], \qquad (10b)$$

where $f(T_m/T)$ is the scaling function, and γ_F depends upon density and is determined by $T_m(\rho)$.

The intuitive basis of the scaling law is the idea that the main effect of interaction between the ions can be summarized in one parameter that measures the interatomic potential at the average ion separation. As this interaction determines the melting temperature, it is no surprise that $T_m(\rho)$

itself serves as a useful scaling parameter.

(3) The *Lindemann melting law*[26] relates the melting temperature $T_m(\rho)$ to the Debye temperature $\Theta_D(\rho)$, which characterizes the quantum effects in low-temperature lattice vibration:

$$T_m(\rho)/\Theta_D^2(\rho) = \alpha/\rho^{2/3}. \tag{11}$$

The constant α depends upon the material but is assumed independent of density and temperature.

(4) The *Dulong–Petit law*[26] is the formula

$$E_i \cong 3kT/AM_p, \tag{12}$$

which applies to solids in a high-temperature range $\Theta_D \ll T \ll T_m$, where lattice vibrations are essentially classical oscillations. In this case the energy per atom is a kinetic energy $\tfrac{3}{2}kT$ plus an equal vibrational potential energy. It should be emphasized that E_i is the ion thermal energy and does not include the work required to compress to the specified density nor electronic excitation energy.

(5) The *Grüneisen pressure law*[9,26] asserts that the ion thermal pressure is given by

$$p_i = \gamma_s(\rho)\rho E_i, \tag{13}$$

where E_i is the ion thermal energy of Eq. (12) and the coefficient γ_s is the solid-phase Grüneisen coefficient.

(6) Another general formula relates the *Grüneisen coefficient* γ_s to the density dependence of the lattice vibration energies,

$$\gamma_s(\rho) = \frac{\partial \log \Theta_D}{\partial \log \rho}. \tag{14}$$

(7) The *Debye lattice theory* is a well-known approximate quantum theory of solid vibrational specific heats in the region $T < \Theta_D$. This theory predicts a low-temperature specific heat proportional to T^3 for nonmetallic solids.

(8) The *Nernst theorem* or third law of thermodynamics is the requirement that the entropy $S(\rho,T)$ approach zero at low temperatures,

$$\lim_{T\to 0} S(\rho,T) = 0. \tag{15}$$

This equation holds for any quantum system having a nondegenerate ground state.

B. Cowan ion EOS

The Cowan ion equation of state is a single analytic model which combines the general relations (1)–(8) given above. The Cowan model can be divided into two parts, a *structural part* which gives the thermodynamic functions p, E, S, and $F = E - TS$ on the basis of assumed expressions for melting and Debye temperatures, and a *phenomenological part* which attempts to predict $T_m(\rho)$ and $\Theta_D(\rho)$ for any material. These two parts are largely independent.

Both structural and phenomenological parts of the Cowan model are very useful without being exact or rigorous. In examining the theory we especially want to observe which equations are interdependent in order to make clear how far one could improve the description of any specific material by altering the Cowan prescriptions for T_m, Θ_D, and γ_s.

C. Structural model

The structural model constructs thermodynamic functions in terms of a known melting temperature $T_m(\rho)$ and Debye temperature $\Theta_D(\rho)$ assumed to obey the Lindemann law, Eq. (11). The *scaling variables* u and w are

$$u = \Theta_D(\rho)/T, \tag{16}$$

$$w = T_m(\rho)/T. \tag{17}$$

As a consequence of Eq. (11) these variables obey

$$w/u^2 = \alpha T/\rho^{2/3}. \tag{18}$$

The solid phase corresponds to the range $w > 1$, and the range $w < 1$ is called the *fluid phase*.

The ion free energy per gram is written

$$F_i(\rho,T) = (kT/AM_p) f(u,w), \tag{19}$$

where, following Cowan, we assume for the fluid phase

$$f = -\frac{11}{2} + \frac{9}{2} w^{1/3} + \frac{3}{2} \log\left(\frac{u^2}{w}\right), \quad w < 1, \tag{20}$$

for the high-temperature solid

$$f = -1 + 3\log u + (3u^2/40 - u^4/2240),$$
$$w > 1, \quad u < 3, \tag{21}$$

and for the low-temperature solid

$$f = \frac{9u}{8} + 3\log(1 - e^{-u}) - \frac{\pi^4}{5u^3}$$
$$+ e^{-u}\left(3 + \frac{9}{u} + \frac{18}{u^2} + \frac{18}{u^3}\right), \quad w > 1, \quad u > 3. \tag{22}$$

These equations define the Cowan structural model in a mathematical sense. In the remainder of this section we explain the physics of Eqs. (20)–(22), show that they reproduce the known limiting cases (1)–(8), and then ask whether the equations can be generalized without significantly changing the structure of the theory.

D. Solid phase

According to Eqs. (21) and (22), the solid-phase ion free energy depends only on $u = \Theta_D/T$, aside from the overall factor (kT/AM_p):

$$F_i(\rho,T) = (kT/AM_p) f(u), \quad w > 1. \tag{23}$$

For a free energy of this form, the ion pressure and energy are

$$p_i = \rho^2 \frac{\partial F_i}{\partial \rho} = \frac{k\rho^2}{AM_p} f'(u) \frac{\partial \Theta_D}{\partial \rho}, \tag{24}$$

$$E_i = -T^2 \frac{\partial}{\partial T}\left(\frac{F_i}{T}\right) = \frac{k\Theta_D}{AM_p} f'(u). \tag{25}$$

The ratio is *independent* of $f(u)$, so that with

$$\gamma_s(\rho) = \frac{\partial \log \Theta_D}{\partial \log \rho},$$

we have

$$p_i = \gamma_s(\rho)\rho E_i.$$

Thus the free energy of Eq. (23) will automatically imply the Grüneisen law, Eq. (13), for any function $f(u)$.

The physical interpretation of the Grüneisen law can be simply paraphrased by recalling that the solid-phase thermal energy is associated with crystal lattice vibrations. According to the Debye theory, the energy E_i belongs to a Bose–Einstein gas of quantized sound waves having an idealized frequency spectrum $g(\nu) = g_0 \nu^2$. Equation (13) then gives the pressure produced by compressing this gas of phonons.

In real materials the phonons have a complicated or density-dependent spectrum $g(\nu)$ and there are corrections to the simple Debye model. For thermodynamic purposes the corrections are usually not large in the range above room temperature.

In the Debye theory the maximum allowed frequency is related to the Debye temperature ($h\nu_D = k\Theta_D$) and the coefficient g_0 is $9/\nu_D^3$, corresponding to three vibrational degrees of freedom per atom. The Helmholtz free energy per atom is then[26]

$$F_{at} = \int_0^{\nu_D} g(\nu)\left(\frac{h\nu}{2} + kT \log(1 - e^{-h\nu/kT})\right) d\nu. \quad (26)$$

Equation (26) includes a zero-point energy $h\nu/2$ per mode.

E. Low-temperature solid

A low-temperature series for Eq. (26) is easily found by integration by parts and expansion in powers of e^{-u}:

$$f(u) = \frac{9u}{8} + 3 \log(1 - e^{-u}) - \frac{\pi^4}{5u^3}$$
$$+ \sum_{n=1}^{\infty} \frac{3}{n} e^{-nu}\left(1 + \frac{3}{nu} + \frac{6}{n^2 u^2} + \frac{6}{n^3 u^3}\right). \quad (27)$$

Equation (22) results from neglecting the (small) terms with $n > 1$. In this approximation

$$f'(u) = \frac{9}{8} + \frac{3}{e^u - 1} + \frac{3\pi^4}{5u^4}$$
$$- e^{-u}\left(3 + \frac{9}{u} + \frac{27}{u^2} + \frac{54}{u^3} + \frac{54}{u^4}\right). \quad (28)$$

The pressure and energy are obtained when this expression is employed in Eqs. (24) and (25). The entropy is $S = -(k/AM_p)(f - uf')$. As $T \to 0$, S approaches zero as T^3, so that the Nernst theorem, Eq. (15), is satisfied. With $f'(\infty) = \frac{9}{8}$, we find the zero-temperature values

$$E_i(\rho, 0) = \frac{9}{8} k\Theta_D / AM_p, \quad (29a)$$

$$p_i(\rho, 0) = \gamma_s \rho E_i(\rho, 0). \quad (29b)$$

These values correspond to the lattice vibration zero-point energy and its (Grüneisen) pressure. The low-temperature specific heat is approximately

$$\frac{dE_i}{dT} \simeq \frac{12\pi^4 k}{5AM_p}\left(\frac{T}{\Theta_D}\right)^3, \quad (29c)$$

a well-known result.[26]

At $u \leqslant 3$ or $T \geqslant \frac{1}{3}\Theta_D$, we will employ the high-temperature expansion formulas. The values implied by Eq. (22) are

$$f(3) = 2.931\,731, \quad f'(3) = 1.422\,887,$$
$$f''(3) = -0.253\,448. \quad (30)$$

F. High-temperature solid

For typical solids the Debye temperature Θ_D is $\simeq 300$ K, so the "high-temperature" case ($u \leqslant 3$) actually means $T \geqslant 100$ K. The great majority of practical applications fall into this range. In this case a power expansion[27] of $f(u)$ gives

$$f(u) = 3 \log u - 1 + \left(\frac{3u^2}{40} - \frac{u^4}{2240}\right) + \frac{u^6}{181\,440}. \quad (31)$$

The final term contributes less than 0.5% and is therefore omitted from Eq. (21). The simplified derivative is then

$$f'(u) = \frac{3}{u} + \left(\frac{3u}{20} - \frac{u^3}{560}\right). \quad (32)$$

At the matching point ($u = 3$) the results from Eq. (21) are

$$f(3) = 2.934\,676, \quad f'(3) = 1.401\,786,$$
$$f''(3) = -0.231\,548. \quad (33)$$

These values indicate a good match with the low-temperature series of Eq. (30) for the thermodynamic functions and their derivatives. If it were considered important one could improve the match by using Eqs. (27) and (31) in place of Eqs. (21) and (22).

Continuing with Eq. (32) for the high-temperature solid, we find

$$E_i = \frac{3kT}{AM_p}\left(1 + \frac{u^2}{20} - \frac{u^4}{1680}\right), \quad (34a)$$

$$p_i = \gamma_s \rho E_i, \quad (34b)$$

$$S_i = (k/AM_p)\left[4 - 3 \log u + \left(\frac{3u^2}{40} - \frac{3u^4}{2240}\right)\right]. \quad (34c)$$

Equation (34a) becomes the Dulong–Petit law in the classical limit ($u \ll 1$). For typical solids at $\rho \simeq \rho_s$, T_m/Θ_D is in the range 2–10 and so $u^2/20 \ll 1$ for $T \simeq T_m$.

The pressure and energy are only weakly dependent on the Debye temperature Θ_D when $u \ll 1$. Evidently one could have a substantial error in Θ_D and still match the experimental equation of state in the high-temperature solid phase as long as the Grüneisen parameter γ_s has a reasonable value.

G. Cowan fluid model

Next we examine the Cowan fluid-phase free energy defined by

$$F_i = (kT/AM_p) f(u, w),$$
$$f(u, w) = -\frac{11}{2} + \frac{9}{2}w^{1/3} + \frac{3}{2}\log(u^2/w).$$

The most interesting aspects of this equation are its match to the solid–phase theory along the melting boundary, $T = T_m(\rho)$; the scaling-law range, where the Debye temperature drops out of the formulas for p and E; and the ideal gas range where neither T_m nor Θ_D explicitly appear in p or E. After examining these features we briefly consider a more general fluid free energy to see whether the Cowan theory can be improved.

The fluid formulas are used for all temperatures $T > T_m(\rho)$ without distinction between liquid and gas phase regions. The gas–liquid phase boundary is introduced later on the basis of a Maxwell construction described in Sec. VII.

The fluid-phase energy, pressure, and entropy resulting from Eqs. (20) are

$$E_i = \tfrac{3}{2}(kT/AM_p)(1 + w^{1/3}), \tag{35a}$$

$$p_i = (\rho kT/AM_p)(1 + \gamma_F w^{1/3}), \tag{35b}$$

$$S_i = (k/AM_p)[7 - 3w^{1/3} + \tfrac{3}{2}\log(w/u^2)], \tag{35c}$$

where

$$\gamma_F = \frac{3}{2}\frac{\partial \log T_m}{\partial \log \rho}. \tag{36}$$

The derivation of Eq. (35b) requires the use of the Lindemann law, Eq. (18).

On the fluid side of the melting curve, $w = 1$ and we have

$$f = -1 + 3 \log u \quad (w = 1). \tag{37}$$

This can be compared to Eq. (31) for the high-temperature solid. Equations (35) simplify for $w = 1$:

$$E_i = 3kT/AM_p, \tag{38a}$$

$$p_i = (\rho kT/AM_p)(1 + \gamma_F), \tag{38b}$$

$$S_i = (k/AM_p)(4 - 3 \log u). \tag{38c}$$

These forms are close to the high-temperature solid forms. The energy and free energy differ only by terms $\simeq u^2/20$, which are not large for most materials at solid density, because

$$\frac{u^2}{20} \simeq \frac{1}{10}\left(\frac{\Theta_D}{T_m}\right)^2 \lesssim 0.01. \tag{39}$$

This quantity is even smaller at higher densities, according to the Lindemann law.

The pressure equation (38b) agrees with (34b) because of the useful formula

$$1 + \gamma_F = 3\gamma_s, \tag{40}$$

which follows from the Lindemann law, Eq. (11).

Comparing Eqs. (34) with (38), we see that liquid-solid phase equilibrium occurs with essentially equal density and temperature; i.e., to the accuracy of the approximation $u^2/20 \ll 1$, there is no volume change on melting, and the Gibbs free energies of the liquid and solid phase match *a fortiori* because both pressures and Helmholtz free energies match. As a consequence there is no latent heat of fusion.

This is a rather schematic description of melting which would not be satisfactory for applications at low pressures where the omitted physics could lead to significant consequences (e.g., the slow movement of glaciers). For high energy-density phenomena (e.g., shock waves generated by meteorite impact upon a glacier), QEOS is probably entirely adequate. A latent heat would appear as a discontinuity in the energy table and this would be somewhat inconvenient.

According to Monte Carlo simulations of fluids with various power-law potentials, the volume change on melting is not large, especially for the Coulomb fluid.[28]

Next we examine the fluid-scaling region of the EOS surface, where both pressure and energy depend on T_m (i.e., w), but not upon the Debye temperature. In effect, all dependence on Θ_D is concealed in the entropy.

The Cowan assumption for the nonideal part of the ion energy is not rigorously correct, but it is surprisingly similar to a known result for the one-component plasma (OCP),[24]

$$\delta E/NkT = a\Gamma + b\Gamma^{1/4} + c. \tag{41}$$

This form approximately fits Monte Carlo simulations of the ion Coulomb fluid. The first term ($a\Gamma \simeq \tfrac{9}{10}Z^2 e^2/R_0 kT$) is a Madelung energy included in the Thomas–Fermi electronic model [see Sec. IV and Eqs. (90) and (91)] and the leading correction is then

$$b\Gamma^{1/4} \simeq 2.95(T_m/T)^{0.25}. \tag{42}$$

In extracting this numerical form, we employ $b = 0.8165$ and $\Gamma_m = 170$.

The OCP results or results for power-law potentials are not rigorously applicable to partially ionized plasmas because in the physical problem the interionic potential is strongly temperature dependent. For this reason a disagreement with Eq. (42) cannot be used as an error estimate for the Cowan model except in a general or qualitative sense. For the Cowan theory Eq. (35a) gives

$$\delta E/NkT = 1.5(T_m/T)^{0.33}. \tag{43}$$

The numbers do not agree but the qualitative similarity is clear. The Cowan form has the special virtue of reproducing Eq. (12) at $T = T_m$.

In the ideal gas range ($w \ll 1$) the Cowan pressure and energy approach the correct limits and the entropy becomes

$$S \to (k/AM_p)[S_1 + \tfrac{3}{2}\log(kT/\rho^{2/3})], \quad T \to \infty. \tag{44}$$

In extracting this form, one again takes advantage of the Lindemann law, Eq. (18). However, the Cowan entropy constant is

$$S_1 = 7 + \tfrac{3}{2}\log \alpha. \tag{45}$$

This reflects the constant α of the Lindemann law and bears no automatic relation to the correct entropy constant of Eq. (9). For example, for high-temperature aluminum, the phenomenological Cowan formulas given below will yield $\alpha \cong 173$ and

$$S_1 = 14.7, \tag{46}$$

while the Sackur–Tetrode law, Eq. (9), gives

$$S_0 = 16.7 \quad (g = 1). \tag{47}$$

Of course the dominant logarithmic term $\tfrac{3}{2}\log(kT/\rho^{2/3})$ in the entropy is correct in the ideal gas range.

In summary, the Cowan fluid model matches thermodynamic functions of the solid phase along the melting curve with negligible latent heat or volume change at melting. It reduces to the ideal EOS at high temperatures ($T \gg T_m$) and between these limits the nonideal part of the EOS is a simple power-law function of the scaling variable $T_m(\rho)/T$.

H. Generalized fluid model

To generalize Eq. (20) we now assume

$$f = \underline{a} + \underline{b}w^{\underline{c}} + \underline{e}\log(u^2/w), \tag{48}$$

where the coefficients $\underline{a}$, $\underline{b}$, $\underline{c}$, and $\underline{e}$ are used only in this section. The scaling variables u and w are still defined as Θ_D/T and T_m/T and assumed to obey the Lindemann relation.

From this free energy one finds

$$E_i = (kT/AM_p)(\underline{e} + \underline{bc}w^{\underline{c}}), \qquad (49a)$$

$$p_i = \left(\frac{\rho kT}{AM_p}\right)\left(\frac{2}{3}\underline{e} + \underline{bc}w^{\underline{c}}\frac{\partial \log T_m}{\partial \log \rho}\right), \qquad (49b)$$

$$S_i = (k/AM_p)[\underline{e} - \underline{a} + \underline{b}(\underline{c} - 1)w^{\underline{c}} + \underline{e}\log(w/u^2)]. \qquad (49c)$$

In order to obtain the correct pressure and energy in the ideal gas limit ($w \to 0$), we must take

$$\underline{e} = \tfrac{3}{2}. \qquad (50)$$

In this limit the entropy constant becomes

$$S_2 = \underline{e} - \underline{a} + \underline{e}\log \alpha. \qquad (51)$$

Next, the energy and pressure will reduce to the solid-phase forms at $w = 1$ if

$$\underline{bc} = \tfrac{3}{2}, \qquad (52)$$

$$1 + \underline{bc}\frac{\partial \log T_m}{\partial \log \rho} = 3\gamma_s, \qquad (53)$$

where the second equation follows from Eq. (40), and the entropy will reduce to the proper value if

$$\underline{a} + \underline{b} = -1. \qquad (54)$$

Thus the limiting cases give three conditions: $\underline{a} + \underline{b} = -1$, $\underline{e} = \underline{bc} = \tfrac{3}{2}$. These requirements are satisfied by the Cowan fluid free energy of Eq. (20). However, we are still free to select $\underline{a}$ in order to obtain a better value for the entropy constant, i.e., to obey Eq. (9b).

If we use an approximate value $\alpha = \tfrac{1}{2}A^{5/3}$ for the Linde-mann constant of Eq. (11) and neglect the nuclear spin entropy ($g = 1$) we find

$$\underline{a} = -8.006, \quad \underline{b} = +7.006, \quad \underline{c} = 0.214, \quad \underline{d} = \tfrac{3}{2}. \qquad (55)$$

These values differ somewhat from the Cowan values and show how much flexibility the approach has. The case for Eq. (55) is not strong enough to justify using them in place of the Cowan forms.

I. Cowan empirical model

In order to use the ion equation of state we need to know the melting temperature T_m, the Debye temperature Θ_D, and the solid-phase Grüneisen coefficient γ_s, not only at the normal solid density, but also as functions of density. Often EOS data is developed on the basis of experimental low-pressure values T_m, Θ_D, and γ_s. This approach faces the difficulty of deciding how the quantities vary with density outside the experimental range. In the Cowan approach, simple formulas are introduced that predict these parameters at any density for any substance.

The predictions of the Cowan formulas are not correct—they could not be when the formulas are so simple—but nevertheless the results have enough connection with reality to reproduce general trends in the periodic table.

It is important to keep in mind that the error of the equation of state is not measured by the error in T_m or Θ_D, but only by the error in total pressure and/or total energy. Analysis of Eq. (35b) shows

$$\frac{\partial \log p_i}{\partial \log T_m} = \frac{1}{3}\frac{\gamma_F w^{1/3}}{1 + \gamma_F w^{1/3}} \simeq \frac{1}{3}, \qquad (56)$$

so that a 30% error in T_m generates only a 10% error in p_i.

Two important properties are assumed by the structural model,

$$\gamma_s = \frac{\partial \log \Theta_D}{\partial \log \rho}, \qquad (57)$$

$$T_m/\Theta_D^2 = \alpha/\rho^{2/3}. \qquad (58)$$

In addition, α is related to the high-temperature entropy constant by Eq. (45).

Following Cowan we define a "reference density,"

$$\rho_{\text{ref}} = (A/9Z^{0.3})\,(\text{g/cm}^3). \qquad (59)$$

This density corresponds to an atomic radius $R_a \approx 1.5 \times 10^{-8}Z^{0.1}$ cm. The actual solid density is compared to ρ_{ref} in order to decide whether the material is loosely or tightly bound; if ρ/ρ_{ref} is large one may expect strong inter-atomic interactions leading to a high melting temperature and conversely. With no additional *a priori* justification, the Cowan formulas for T_m, Θ_D, and γ_s are

$$kT_m = 0.32[\xi^{2b+10/3}/(1+\xi)^4]\ (\text{eV}), \qquad (60)$$

$$k\Theta_D = [1.68/(Z+22)][\xi^{b+2}/(1+\xi)^2]\ (\text{eV}), \qquad (61)$$

$$\gamma_s = b + 2/(1+\xi). \qquad (62)$$

Here $b = 0.6Z^{1/9}$ is a constant for any given element and $\xi = \rho/\rho_{\text{ref}}$. The reader can easily verify that these formulas satisfy Eqs. (57) and (58) with

$$\alpha = 0.0262(A^{2/3}/Z^{0.2})(Z+22)^2. \qquad (63)$$

We can evaluate the Cowan formulas by testing them against data for elements at the normal solid density and with theories that apply at strong compressions ($\xi \to \infty$).

Figures 4 and 5 compare T_m and Θ_D for elemental solids with the Cowan predictions. There are significant disagreements, especially for transition metals. Nevertheless, the Cowan formulas do a remarkable job of following trends
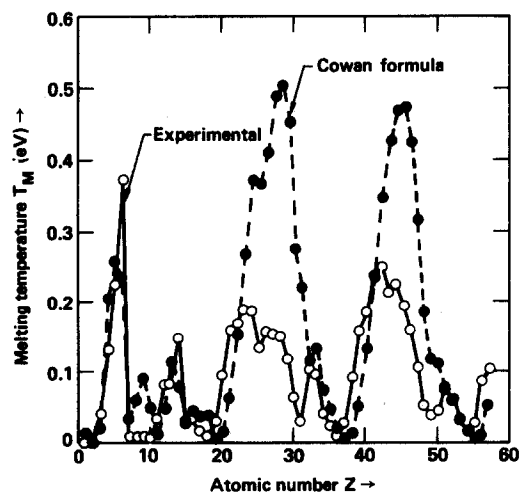

FIG. 4. Melting temperatures of elements at their normal densities. The Cowan formula appears to follow the main trends in the periodic table while overestimating T_M for transition metals.
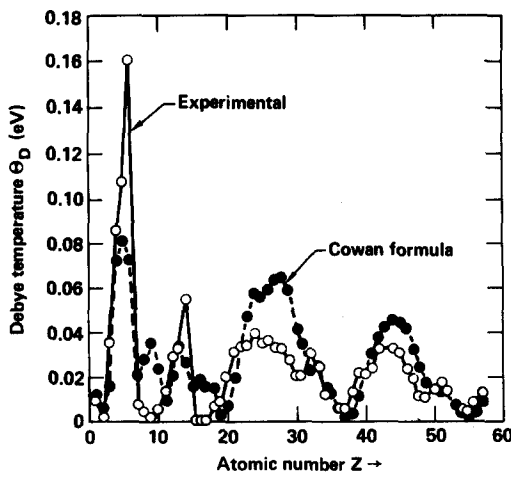
FIG. 5. Debye temperatures of the elements. The Cowan model nicely follows the trends of the periodic table despite substantial disagreements for certain materials.

FIG. 7. Ratio of the solid-density melting temperature and (squared) Debye temperature, as appears in the Lindemann law, for various elements.

in the periodic table which we attribute to the strong chemical correlation between solid density, bond strength, and the characteristic temperatures T_m and Θ_D.

Figures 6 and 7 compare the solid-density Grüneisen coefficient $\gamma_s (\rho_s)$ and the Lindemann ratio α to available experimental data.[29] In this case there is little systematic pattern in the experimental data, aside from the rough statements $1 \lesssim \gamma_s < 2.5$ and $0.25 < \alpha < 1$. The Cowan values show systematic (but incorrect) dependence on atomic number.

The disagreements shown in Figs. 6 and 7 are more important than those seen in Figs. 4 and 5; if γ_s is sufficiently wrong it becomes difficult to match shock-wave data.

Finally Fig. 8 compares the Cowan Grüneisen coefficient $\gamma_s (\rho)$ for aluminum to a Thomas–Fermi calculation of Kopyshev. The theoretical curve approaches $\gamma = \frac{1}{2}$ at extreme high densities. The TF value at the normal solid density is not especially correct; in general, Thomas–Fermi theory gives a poor description of solid-density matter because it omits the energy associated with chemical bonding.

J. Improved empirical model

It is not difficult to generalize the simple formulas given in Eqs. (60)–(62) while preserving the important properties required by the structural model, i.e., Eqs. (57) and (58). We assume

$$\gamma_s = \mu/(1 + \xi) + \nu, \tag{64}$$

$$\Theta_D = \lambda \rho_r^\nu \xi^{\mu + \nu}/(1 + \xi)^\mu, \tag{65}$$

$$T_m = \alpha \lambda^2 \rho_r^{2\nu - 2/3} \xi^{2(\mu + \nu - 1/3)}/(1 + \xi)^{2\mu}. \tag{66}$$

We can then determine μ, ν, and λ by requiring that $\gamma_s (\rho_s)$ be acceptable, that $\gamma_s \to \frac{1}{2}$ as $\rho \to \infty$ (i.e., $\nu = \frac{1}{2}$), and that $T_m (\rho_s)$ be reasonable. The ultimate high-density limit of T_m is also known, however. From the OCP model one has (assuming $\Gamma_{melt} \cong 170$)

$$kT_m \approx 0.115(Z^2 \rho^{1/3}/A^{1/3}) \ (eV), \quad \rho \to \infty. \tag{67}$$

One wants to end with a predicted melting temperature not too far from this value in the extreme high-density limit.

For example, if one must raise $\gamma_s (\rho_s)$ to match Hugoniot data, it is better to do this by raising μ rather than ν to avoid an extremely high melting temperature at high
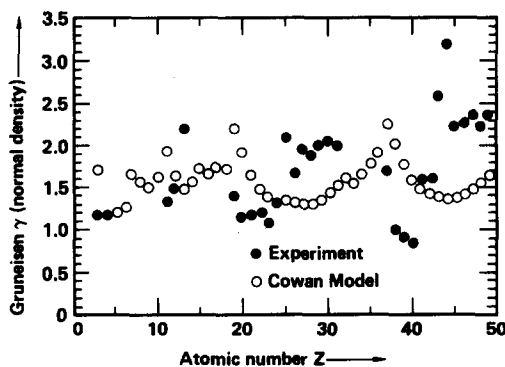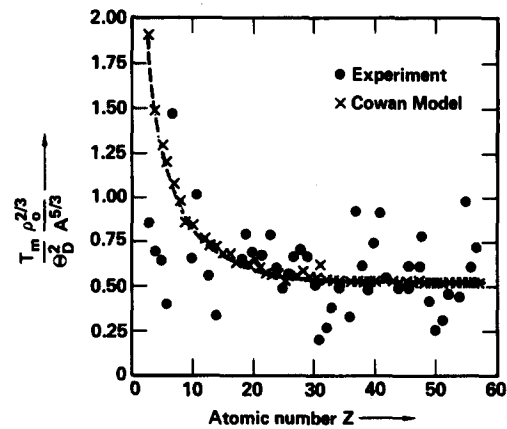

FIG. 6. Grüneisen parameters for elements at their normal solid densities. In this case the Cowan formulas introduce a spurious periodicity in $\gamma(Z)$. There is more difficulty fitting an equation of state if the Cowan γ is significantly below the experimental value.
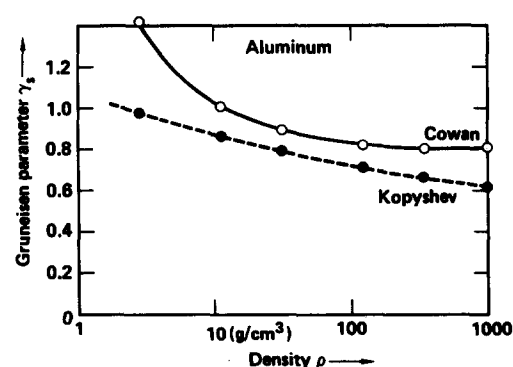

FIG. 8. Density dependence of the Grüneisen parameter $\gamma_s (\rho)$. The dashed curve is based on Thomas–Fermi lattice dynamics calculations of Kopyshev and may be considered to be correct at extreme high densities (above 100 g/cm³). The Cowan value is more accurate near normal density.

density. Such a value would have little effect on the normal density EOS but would cause the degenerate adiabats to have unrealistic curvature.

IV. ELECTRON EQUATION OF STATE

Feynman, Metropolis, and Teller[2] formulated a Thomas–Fermi theory of hot dense plasmas in terms of the spherical-cell model for compressed atoms, a physical description which has proven extraordinarily fruitful. In QEOS we employ this original TF cell model with improved numerics but without exchange or other corrections. This choice is reasonable because the scaling property of the uncorrected Thomas–Fermi theory is a major practical advantage, and because the semiempirical modifications described in Secs. V and VI are able to correct the quantitative deficiencies in the Thomas–Fermi results, at least to the accuracy required for hydrodynamic applications.

A. Basic Thomas–Fermi equations

In Thomas–Fermi theory the electrons are treated as a charged fluid surrounding the nucleus; properties of this electron gas are obtained from finite-temperature Fermi–Dirac statistics. Effects of the plasma environment are introduced by the *ion-sphere model*: each nucleus is located at the center of a spherical cavity of radius $R_0 = (3/4\pi n_i)^{1/3}$; the cavity contains enough electrons to be electrically neutral and other ions are assumed to remain outside the sphere.

Within the ion sphere, an electrostatic potential $V(r)$ is calculated by solving the Poisson equation,

$$\nabla^2 V = 4\pi e n(r) - 4\pi Z e \delta(\mathbf{r}) . \tag{68}$$

Here $n(r)$ is the total electron number density which includes both bound and free electrons. At the origin, $V(r) \to Ze/r$, the nuclear potential. Neutrality of the ion sphere implies

$$\frac{\partial V}{\partial r} = 0 , \tag{69}$$

at $r = R_0$. The zero of electron single-particle energy is normally chosen such that $V(R_0) = 0$.

The electron density $n(r)$ is determined by the formula for a finite-temperature semiclassical electron gas,

$$n(r) = \int \frac{2 d^3 p}{h^3} f(r,p) = c_1 (kT)^{3/2} F_{1/2}\left(-\frac{\mu + eV(r)}{kT} \right), \tag{70}$$

where

$$f(r,p) = \{1 + \exp[p^2/2m - eV(r) - \mu]/kT\}^{-1} , \tag{71}$$

$$c_1 = (1/2\pi^2)(2m/\hbar^2)^{3/2} , \tag{72}$$

$$F_\nu(y) = \int_0^\infty \frac{x^\nu \, dx}{1 + \exp(x + y)} . \tag{73}$$

Here $f(r,p)$ is the Fermi–Dirac distribution function. The electron chemical potential μ is determined by the requirement that the cell be neutral,

$$\int n(r) d^3 r = Z . \tag{74}$$

This condition is equivalent to Eq. (69).

The potential $V(r)$ carries the (spherically averaged) electrostatic interaction between electrons. The potential $V(r)$ is *self-consistent*: it must simultaneously satisfy both Eqs. (68) and (70). Equation (70) allows for thermal excitation (and ionization) of the bound electrons, although electron states are not quantized but instead simply represented by their classical phase-space density.

Thomas–Fermi theory includes a surprisingly complete list of plasma density effects.[13] Plasma-ion correlation enters through the ion-sphere model which is reasonably accurate in dense plasmas where the correlation parameter $\Gamma = Q^2 e^2 / R_0 kT$ is large. Free electrons are allowed to be degenerate and also experience the electrostatic potentials of neighbor ions, although this is slightly hidden by the conventional choice $V(R_0) = 0$. The free electrons are not spatially uniform; their density is calculated self-consistently. At high density the free electrons are forced into the ion core and the potential $V(r)$ includes the resulting screening of bound electrons by frees. In Thomas–Fermi calculations the core electrons are pressure ionized at high densities and this process is a smooth (continuous) function of density.

B. Thermodynamic functions

Thomas–Fermi theory is sufficiently well known that we need only summarize the equations actually used in constructing the thermodynamic functions. The kinetic and electrostatic energies (per atom) are given by

$$K = c_1 (kT)^{5/2} \int F_{3/2}\left(-\frac{\mu + eV(r)}{kT} \right) d^3 r , \tag{75}$$

$$U_{en} = -\int \frac{Ze^2}{|r|} n(r) d^3 r , \tag{76}$$

$$U_{ee} = \frac{e^2}{2} \int \frac{n(r)n(r')}{|r - r'|} d^3 r \, d^3 r' . \tag{77}$$

The thermodynamic energy, free energy, and entropy per gram are

$$E_e = (K + U_{en} + U_{ee}) A M_p , \tag{78}$$

$$F_e = (Z\mu - \tfrac{2}{3}K - U_{ee})/A M_p , \tag{79}$$

$$S_e = (\tfrac{5}{3}K - Z\mu + U_{en} + 2U_{ee})/(A M_p T) , \tag{80}$$

where $A M_p$ is the mass per atom. The pressure is

$$p_e = \tfrac{2}{3} c_1 (kT)^{5/2} F_{3/2}(-\mu/kT) . \tag{81}$$

The charge state $Q(\rho, T)$ is taken to be

$$Q = (4\pi/3) R_0^3 n(R_0) . \tag{82}$$

In the literature one sometimes finds an alternative definition of Q based on integration of $f(r,p)$ over states of positive energy. In fact, two closely analogous definitions of Q can be formulated for the quantum average-atom model; in that case the difference is mainly due to electrons in resonance states confined by the centrifugal barrier but at positive energy.[30] For applications such as the evaluation of conduction

coefficients, the simple formula (82) is probably most appropriate.

C. TF scaling

The scaling law relates properties of an arbitrary element (atomic number Z, atomic weight A) to those defined by the case $Z = A = 1$. We assume the arbitrary material has density ρ and temperature T, and define

$$\rho_1 = \rho/AZ , \tag{83a}$$

$$T_1 = T/Z^{4/3} . \tag{83b}$$

The scaling is then expressed by the equations

$$Q(Z,\rho,T) = ZQ_1(\rho_1,T_1) , \tag{84a}$$

$$p(Z,\rho,T) = Z^{10/3}p_1(\rho_1,T_1) , \tag{84b}$$

$$\mu(Z,\rho,T) = Z^{4/3}\mu_1(\rho_1,T_1) , \tag{84c}$$

$$E(Z,\rho,T) = (Z^{7/3}/A)E_1(\rho_1,T_1) , \tag{84d}$$

$$S(Z,\rho,T) = (Z/A)S_1(\rho_1,T_1) , \tag{84e}$$

$$F(Z,\rho,T) = (Z^{7/3}/A)F_1(\rho_1,T_1). \tag{84f}$$

These equations apply only to the Thomas–Fermi electron contributions to pressure, energy, etc. The formulas are proven by change of variables (e.g., $r \to r_1/Z^{1/3}$) in Eqs. (68)–(81).

The practical significance of the scaling property is that a single table of $F_1(\rho_1,T_1)$ provides thermodynamic data for any element (mixtures are discussed below). If we used the Thomas–Fermi–Dirac (TFD) or quantum statistical model (QSM) theories, which are more accurate than the TF theory, we would have to give up this scaling property; at present this is not an attractive option.

The scaling property relates plasmas at the very different apparent conditions. For example, a plasma of Au ($Z = 79$) at $\rho = 0.1$ g/cm^3, $T = 100$ eV translates to $\rho_1 = 6.4 \times 10^{-6}$ g/cm^3, and $T_1 = 0.29$ eV. For this reason we need a wide-range table of $F_1(\rho_1,T_1)$ which reaches densities and temperatures that would seem very low for the case $Z = A = 1$.

D. Numerical tests

The TF scaling property causes some numerical difficulties because the ion core region contains a substructure capable of imitating the K shell of much heavier ions and this substructure must be fully resolved. The numerical calculations can be verified by a series of tests.

(1) Zoning. Our code integrates by Simpson's rule with fine zoning near $r = 0$ and additional end point corrections for the singular behavior at small radii where

$$n_{TF}(r) \cong \frac{1}{3\pi^2}\left(\frac{2Z}{a_0 r}\right)^{3/2}\left[1 + 0\left(\frac{Z^{1/3}r}{a_0}\right) + \cdots\right] \tag{85}$$

($a_0 = \hbar^2/me^2$ is the Bohr radius). The numerical test is to verify explicitly convergence with respect to the number of zones.

(2) Virial theorem. A nontrivial check of the overall numerical accuracy of the calculation is the equation

$$3p[(4\pi/3)R_0^3] = 2K + U_{en} + U_{ee} . \tag{86}$$

At most ρ,T conditions, our code satisfies this equation to high precision.

(3) Z scaling. Equations (84) give another check on the numerical calculations.

(4) Nernst theorem. As $T \to 0$ the entropy should vanish. This gives a formula

$$Z\mu = \tfrac{5}{3}K + U_{en} + 2U_{ee} \quad (T = 0) , \tag{87}$$

which tests the $T = 0$ calculation.

(5) Numerical derivatives. Pressure and entropy can be calculated as numerical derivatives,

$$p = \rho^2\frac{\partial F}{\partial \rho} , \tag{88}$$

$$S = -\frac{\partial F}{\partial T} . \tag{89}$$

These derivatives should agree with Eqs. (80) and (81).

(6) Limiting cases. In Sec. IV E we describe three limiting cases that are important in defining the table representation because we want our interpolation scheme to be able to correctly reproduce (at least) these limits. The limiting cases are described by Eqs. (90)–(92) which also test the code.

The TF code used in our calculations passes these tests to high precision and in most cases the results are accurate to five figures. Because the code was to be run many times (the TF table described below has $79 \times 64 = 5056$ entries), we devised a powerful new method for the rapid solution of self-consistent field equations (see the Appendix).

E. Limiting cases

At very high temperature we expect to encounter a (nearly) fully ionized ideal gas for which the free energy per atom is

$$F_e = ZkT\left[-1 + \log\left(\frac{Z\rho\lambda_e^3}{2AM_p}\right)\right] - \frac{9}{10}\frac{Z^2e^2}{R_0} . \tag{90}$$

Here $\lambda_e = (h^2/2\pi mkT)^{1/2}$ is the electron thermal de Broglie wavelength. The second term is the Madelung energy ($U_{en} = -\tfrac{3}{2}Z^2e^2/R_0$, $U_{ee} = \tfrac{3}{5}Z^2e^2/R_0$) of Z free electrons uniformly distributed over the ion-sphere volume. (In discussing the ion EOS we remarked that this energy appears in the TF electron EOS.)

At very high density and low temperature the TF theory yields a degenerate homogeneous electron gas interacting with the ion cores. In this case

$$F_e = E_e = \frac{3}{5}\frac{\hbar^2}{2m}\left(3\pi^2\frac{Z\rho}{AM_\rho}\right)^{2/3}Z - \frac{9}{10}\frac{Z^2e^2}{R_0} . \tag{91}$$

This is independent of T and corresponds to complete pressure-induced ionization.

The third known limit occurs at low density, if the limit $T \to 0$ is taken first. In this case one has a gas of neutral TF atoms with a binding energy independent of both density and temperature, given by

$$F_e = E_e = -0.768745\,Z^{7/3}e^2/a_0 . \tag{92}$$

These limiting cases provide checks of the code. The

leading corrections to the asymptotic formulas depend on unphysical properties of the TF ion-core region.

F. Defects of Thomas–Fermi theory

We now examine some defects of the TF theory in order to decide what corrections will be required to obtain a satisfactory general-purpose equation of state. From the outset we propose to ignore purely conceptual questions: obviously Thomas–Fermi theory omits relativistic and quantum effects aside from semiclassical phase-space quantization and Fermi statistics in Eq. (70). For hydrodynamic applications the omitted effects are important only insofar as they change the thermodynamic results.

We review corrections to the TF description of K-shell electrons and quantum shell-closure effects; the chemical physics of valence electrons; exchange, gradient and correlation corrections; and finally the limitation to equilibrium (LTE) states.

G. *K*-shell density

In nonrelativistic quantum calculations the K-shell electron density takes the form

$$n_K(r) = p_K(\alpha^3/8\pi)e^{-\alpha r}, \quad \alpha = 2Z/a_0. \tag{93}$$

Here p_K is the population of the K shell. This charge density is nonsingular (finite) at $r \to 0$, unlike the Thomas–Fermi result in Eq. (85). However the integral of Eq. (85), say from $r = 0$ to $r = a_0/Z$, is a finite number of order unity.

The difference between Eqs. (85) and (93) introduces a correction to the total energy of order[31]

$$\delta E_K \simeq \tfrac{1}{2}Z^2(e^2/a_0) \tag{94}$$

For thermodynamic applications this *Scott correction* is not very useful because the existing theory refers to the isolated atom, and the density-temperature dependence of δE_K is not yet known.

Because the TF electron density (85) is so different from Eq. (93) we must be skeptical of Thomas–Fermi predictions for low-Z elements, where $1s$ and $2s$ electrons play the dominant role.

H. Quantum shell effects

Quantum ionization calculations based on the Saha equation or the quantum average-atom model generally agree with Thomas–Fermi results, although one finds oscillatory modulations of the pressure, energy, etc. around the smooth TF curves. The modulations originate in quantum shell structure, i.e., the discontinuity in ionization potentials which occurs between shells defined by the principal quantum number. For example closed-shell ions (ground state He-like, Ne-like, etc.) are more strongly bound than predicted by Thomas–Fermi theory and therefore occur over a larger temperature range. The amplitude of the shell oscillation is typically not large (perhaps a 10% correction to pressure or energy).[13,21]

A characteristic general rule is that shell oscillations become less prominent at higher densities. This happens because there is a much higher degree of thermal excitation at higher densities; averaging over a large number of excited states greatly smooths the effective ionization potential.[21]

I. Cold-compression curve

The most important defect of the Thomas–Fermi theory is its failure to describe attractive (bonding) forces between neutral atoms. These forces originate in quantum aspects of the electron–electron interaction omitted from the Thomas–Fermi self-consistent field description. The TF theory predicts a monatomic state without chemical bonding either in the molecular gas phase or the solid phase; in particular solid-density matter is incorrectly predicted to have large positive pressures in the Mbar range (see Fig. 9).

This problem is solved by phenomenological methods described in Sec. V.

J. Exchange, gradient, and correlation

Improved versions of Thomas–Fermi theory, known as TFD, Thomas–Fermi–Kirzhnits, (TFK), and QSM theories include various corrections, each of order 10%. For example, the TFD theory adds to the TF theory the electron exchange interaction, calculated in a local-density approximation. The TFK theory adds the first gradient correction to the TF expression for the electron kinetic energy, treating this correction by a perturbation method. In the QSM, these terms are treated self-consistently. In addition one can add a local-density approximation to the electron correlation energy.[12,13,32]

The improved theories are more accurate than the TF theory, but not enough to remove the need for empirical modifications of the type described in Secs. V and VI. In fact, a minor change in the bonding correction of Sec. V will make a TF-based EOS look very much like TFD-based calculations.

This is illustrated in Fig. 9 which shows five calculations of the cold compression of aluminum: Thomas–Fermi (TF)
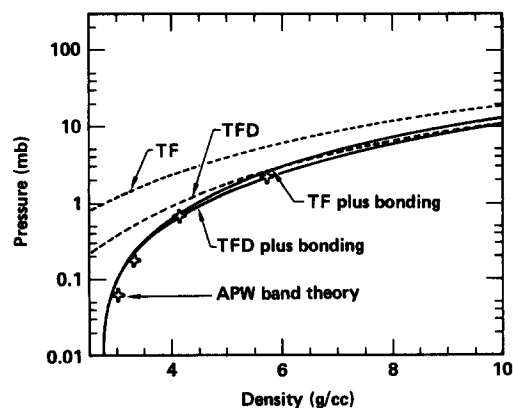
FIG. 9. This picture shows why QEOS is based on the TF electron EOS. The crosses are taken from complete APW electron band-structure calculations of $p(\rho_0)$ for aluminum, and are presumably the best available data. The TF and TFD results, shown as dashed curves, are significantly in error near $\rho_s = 2.7$ g/cm^3, although the TFD theory is more accurate. However, QEOS corrects the TF theory with the bonding correction described in Sec. V, to a result very close to the APW calculations. The bonding-corrected TF is within 10% of the corrected TFD theory; i.e., the difference between TF and TFD is largely absorbed by the bonding correction.

and TFD results, the result of adding appropriately determined bonding corrections and a quantum calculation.[33] While the TF and TFD results differ by a factor of 3 at solid density, the corrected complete equations of state agree there (the bonding correction is of course determined by known properties of the solid); in general the two corrected equations of state agree to within 10%.

In practice we find that the empirical corrections of Secs. V and VI function most reliably when they reduce the pressure, so that the method operates in a robust and trouble-free fashion when applied to the TF electronic EOS. For this reason, and because the corrected statistical theories do not share the TF scaling property, we have chosen to base QEOS on the simpler TF equation of state.

K. LTE restriction

The equation of state produced by the QEOS code will apply only to plasmas in ionization equilibrium, or local thermodynamic equilibrium (LTE). This condition can fail in situations where the radiation and free electron distributions are constrained to have different temperatures. For example, in an optically thin low-density plasma, radiation escapes corresponding to an effective radiation temperature near zero. Then radiative recombination is not balanced by photoionization and the plasma is less ionized than an equilibrium plasma of equal electron temperature.

When effects of this character are important it will be necessary to solve atomic rate equations and derive an approximate EOS from their solution. This problem has not been solved, and it remains an important project for future research.

L. Thomas–Fermi table

Although the Thomas–Fermi theory is relatively simple, it is not practical to evaluate thermodynamic variables with a direct in-line calculation; therefore we tabulate the TF free energy. The scaling law then allows us to obtain the EOS for any element by scaling from a single TF table defined for the case $Z = A = 1$.

Although our applications cover a range of perhaps 6–8 decades in density, centered at 1 g/cm^3, and 3–5 decades in temperature (i.e., 0.1–10 keV), the Thomas–Fermi table for F_1 covers a much larger range in order to include these conditions for all elements.

Interpolation in the TF table is designed to reduce to correct forms in extreme degenerate and nondegenerate limits. The functions used provide for continuity of energy, entropy, pressure, and dp/dT across the table box boundaries. This is accomplished by defining the new quantities

$$u = \rho^{-2/3} , \tag{95}$$

$$H(u,T) = uF = u(E - TS) , \tag{96}$$

for which it follows that

$$\frac{\partial H}{\partial T} = -uS , \tag{97}$$

$$\frac{\partial H}{\partial u} = F - \frac{3}{2} \frac{p}{\rho} , \tag{98}$$

$$\frac{\partial^2 H}{\partial u \, \partial T} = -S - \frac{3}{2\rho} \left(\frac{\partial p}{\partial T} \right)_\rho . \tag{99}$$

Here H and these three derivatives are determined at each point of the table from the Thomas–Fermi code calculations. Within any table box, we use the four quantities evaluated at the box corners to determine the 16 unknowns in the following interpolation function for H:

$$H(u,T) = A(u) + B(u)T + C(u)T^2 + D(u)T \log T , \tag{100}$$

$$A(u) = A_a + A_b u + A_c u^2 + A_d u \log u , \tag{101a}$$

$$B(u) = B_a + B_b u + B_c u^2 + B_d u \log u , \tag{101b}$$

$$C(u) = C_a + C_b u + C_c u^2 + C_d u \log u , \tag{101c}$$

$$D(u) = D_a + D_b u + D_c u^2 + D_d u \log u . \tag{101d}$$

This form is able to reproduce both degenerate and nondegenerate ideal gas limits.

The fitting is done very efficiently by breaking it into several one-dimensional fits. The interpolation function is in effect a bicubic spline with the cubic term replaced by $x \ln x$.

To handle the rare cases when T and/or u lie outside the table, we establish *extrapolation boxes* at the table perimeter in which

$$H = H_0 + uB(T) + u^2 C(T), \quad u \to 0 , \tag{102a}$$

$$= uB(T) + D(T)u \ln u, \quad u \to \infty , \tag{102b}$$

$$= A(u) + C(u)T^2, \quad T \to 0 , \tag{102c}$$

$$= A(u) + B(u)T - \tfrac{3}{2} uT \ln T, \quad T \to \infty . \tag{102d}$$

The constant $H_0 = \tfrac{3}{2} u E_f$ and $E_f \propto \rho^{2/3}$ is the Fermi energy of fully ionized electrons. In the QEOS subroutine the degree of ionization is calculated from the TF pressure by using fits to the Fermi–Dirac integrals.

M. Mixtures

In our work we use a well-known rule for Thomas–Fermi mixing of elements. An initial guess is made of the densities ρ_j of the individual elements in the mixture, and the TF pressures are then calculated. The mean value p of the pressures is chosen and the densities ρ_j are then scaled so that all TF atoms have this pressure,

$$p_j(\rho_j, T) = p . \tag{103}$$

The total density ρ' at this pressure is given by the additive volume rule,

$$\frac{\overline{A}}{\rho'} = \sum_j x_j \frac{A_j}{\rho_j} , \tag{104}$$

where x_j is the number fraction of species j and $\overline{A} = \Sigma_j x_j A_j$ is the mean atomic weight.

The computed density ρ' is then compared with the input density ρ and the ρ_j's are scaled to make $\rho' = \rho$. These densities are then used in a new pressure calculation and the cycle is repeated until $\rho' = \rho$ and all atomic pressures are equal. The appropriate combination of free energies is finally used to compute all other thermodynamic functions for the mixture.

3071   Phys. Fluids, Vol. 31, No. 10, October 1988

More *et al.*   3071

In constructing the complete EOS for a mixture of elements, this mixing rule is applied only to the Thomas–Fermi portion of the EOS. The ion and bonding corrections are handled as if one has a single species of atomic number $\bar{Z} = \Sigma_j x_j Z_j$.

The entropy of mixing is not correctly calculated here, but the entropy is not exact even for a single element, and the error has no effect on normal hydrodynamics.

V. CORRECTION FOR CHEMICAL BONDING

Thomas–Fermi theory gives a positive pressure produced by the gas of free electrons. For metallic electron densities this will be a few megabars at zero temperature. In reality, for cold matter near the normal solid density, chemical bonds support a finite matter density at *zero* total pressure. In order to obtain an approximately correct equation of state for this region, we add a semiempirical bonding correction to the energy:

$$E_b = E_0 \{ 1 - \exp b \, [1 - (\rho_s/\rho)^{1/3}] \} , \qquad (105)$$

where ρ_s is the normal solid density and E_0 and b are positive numbers which characterize the bond strength and range; these two parameters are used only in this section. The energy $E_b(\rho)$ is $\simeq E_0 > 0$ at very low density, is zero at solid density, and becomes constant $\simeq -E_0 [\exp(b) - 1]$ at high density where the Thomas–Fermi energy rises rapidly. In QEOS the bonding energy is taken to be independent of temperature, and therefore Eq. (105) also gives the correction to the Helmholtz free energy.

The convenient functional form of Eq. (105) was introduced by Barnes[3] on the basis of its similarity to the attractive term in the well-known Morse potential.

The bonding correction to the pressure is

$$p_b = \rho^2 \frac{\partial E_b}{\partial \rho} = - \left(\frac{E_0 b \rho_s}{3} \right) \left(\frac{\rho}{\rho_s} \right)^{2/3} \exp b \left[1 - \left(\frac{\rho_s}{\rho} \right)^{1/3} \right] . \qquad (106)$$

At very high density this is much less than $p_e \sim \rho^{5/3}$. The parameters E_0 and b are determined by requiring that the total pressure and bulk modulus be correct for the initial cold solid. The experimental bulk modulus is required to be

$$B = \rho \left(\frac{\partial p_{\text{TOT}}}{\partial \rho} \right)_{\rho_s} = \rho \left(\frac{\partial p_e}{\partial \rho} + \frac{\partial p_i}{\partial \rho} \right)_{\rho_s} - (b+2) \frac{E_0 b \rho_s}{9} . \qquad (107)$$

This equation, together with the requirement that

$$p_{\text{TOT}} (\rho_s, 0) = 0 , \qquad (108)$$

will determine E_0 and b. With a correct bulk modulus, the Barnes correction brings the TF theory into reasonably good agreement with high-pressure shock-wave data for most materials.

In Fig. 9 we have seen that the bonding correction also has the ability to imitate the effects of the exchange energy to an overall accuracy of about 10%.

VI. TEMPERATURE-DEPENDENT PRESSURE MULTIPLIERS

It is useful to have an additional capability to modify the equation of state given by the theory without sacrificing the desirable qualities of smoothness and thermodynamic consistency. In particular, this will enable us to match experimental data for a larger variety of materials. Modifications are typically necessary for materials with solid–solid phase transitions or materials which evaporate to a diatomic molecular gas which remains stable at temperatures of interest. Deuterium–tritium fusion fuel is the most important example.

Given the total free energy $F(\rho,T)$ and the resulting pressure $p(\rho,T)$, energy $E(\rho,T)$, and entropy $S(\rho,T)$, we define a modified free energy $\widetilde{F}(\rho,T)$ as

$$\widetilde{F}(\rho,T) = f(T) F(\rho,T) , \qquad (109)$$

where $f(T)$ is the *temperature-dependent pressure multiplier*, whose name is justified by

$$\tilde{p}(\rho,T) = f(T) p(\rho,T) . \qquad (110)$$

Equation (110) is obtained by forming $\tilde{p} = \rho^2 (\partial \widetilde{F}/\partial \rho)$. Similarly

$$\widetilde{S} = - \frac{\partial \widetilde{F}}{\partial T} = (f + Tf') S - f'E , \qquad (111)$$

$$\widetilde{E} = \widetilde{F} + T\widetilde{S} = (f - Tf') E + T^2 f'S . \qquad (112)$$

The modified pressure $\tilde{p}$, energy $\widetilde{E}$, and entropy $\widetilde{S}$ are obtained from $\widetilde{F}$ by the usual thermodynamic relations, and consequently they obey the condition of thermodynamic consistency. However, we must also ask whether they are satisfactory in other respects.

For example, we must require $f(T) > 0$ at all T to have $\tilde{p} > 0$. Unless $f'(0) = 0$, the entropy will not necessarily obey the Nernst theorem $\widetilde{S}(\rho,0) = 0$ except at solid density where we impose the condition $E(\rho_s,0) = 0$. A more important question concerns the modified specific heat $\widetilde{C}_v = \partial \widetilde{E}/\partial T$,

$$\widetilde{C}_v = fC_v - Tf''E + (2f' + Tf'') TS . \qquad (113)$$

At low temperatures TS and C_v are both small and evidently $f'' < 0$ will guarantee $\widetilde{C}_v > 0$. At high temperatures TS exceeds E and in this case one would like to require $f' > -\frac{1}{2} Tf'' > 0$.

These constraints can be satisfied by various functional forms for $f(T)$ such as

$$f(T) = f(\infty) - \alpha \exp [- (T/T_0)^\beta] , \qquad (114)$$

$$f(T) = f(\infty) - \alpha/(T + T_0)^\beta . \qquad (115)$$

In the second case, the more important constraints on $f(T)$ are fulfilled if

$$\alpha > 0, \quad 0 < \beta < 1, \quad f(\infty) \geqslant \alpha/T_0^\beta . \qquad (116)$$

We find that it is unsatisfactory to mechanically rely on these tests; in order to have a clear idea what the pressure multiplier has done it is important to plot and examine the complete EOS, with special attention to the adiabats. Normally we assume $f(\infty) = 1$ and become nervous if the data seems to require $f(0) < 0.5$; when the basic QEOS Hugoniot falls below the experimental data it appears wiser to return to the ion EOS and raise the Grüneisen parameter rather than using a decreasing pressure multiplier that violates Eq. (116).

For molecular compounds such as H_2, O_2, N_2, etc., our monatomic ion EOS predicts roughly twice the correct pres-

sure at low temperatures. The discrepancy can be expected to disappear as one reaches temperatures where the molecules dissociate. Rather than solve this problem by improvement of the ion EOS, it is more expedient to simply introduce a pressure multiplier with $f(0) = 0.5$, which rises to unity above temperatures of 1–5 eV.

The use of a low-temperature pressure multiplier $f(0) < 1$ also requires a compensating increase in the input bulk modulus used in Eq. (107) in order to end with the correct total EOS.

Another application possible with in-line use of the QEOS subroutine is to test sensitivities of a hydrodynamic calculation to EOS uncertainties at specified temperature conditions. For this, one closely compares a nominal calculation with $f = 1$ to a modified calculation using $f = 1 \pm 0.2$ in a selected temperature range. This comparison would be difficult to perform with a fixed tabular EOS.

VII. LIQUID–VAPOR PHASE EQUILIBRIUM

QEOS, like other statistical–mechanical theories based on the Helmholtz free energy, gives unphysical van der Waals loops in the liquid–vapor two-phase region. Since the two-phase region disappears in a critical point with a temperature typically less than 1 eV, this feature of the model is not important for hot plasma applications and usually may be ignored. For certain applications where the low-temperature range is important, we eliminate the loops and replace them with a realistic liquid–vapor equation of state. This is the standard procedure when QEOS is used to construct a library equation of state table.

The first step in eliminating the loops is to locate the *critical point* defined by

$$\frac{\partial p}{\partial \rho} = 0 , \tag{117}$$

$$\frac{\partial^2 p}{\partial \rho^2} = 0 . \tag{118}$$

This pair of equations is solved by an iterative scheme. Then for each chosen temperature $T < T_c$, the maximum and minimum pressure of the loop are found and an iterative search is made for an intermediate pressure that satisfies the conditions

$$G_v = G_l , \tag{119}$$

$$p_v = p_l , \tag{120}$$

$$T_v = T_l . \tag{121}$$

Here G is the Gibbs free energy and v and l refer to vapor and liquid, respectively. The resulting pressure is the equilibrium liquid–vapor pressure, $p_{eq}(T)$. The procedure is indicated in Fig. 10, and a typical liquid–vapor coexistence region is shown in Fig. 1.

The result of these calculations is a table containing T, p, $\rho_v, \rho_l, E_v,$ and E_l, where E is the internal energy. For construction of the EOS table of $p(\rho,T)$ and $E(\rho,T)$, QEOS is evaluated as usual for points outside of the coexistence region. Inside the region, one forms
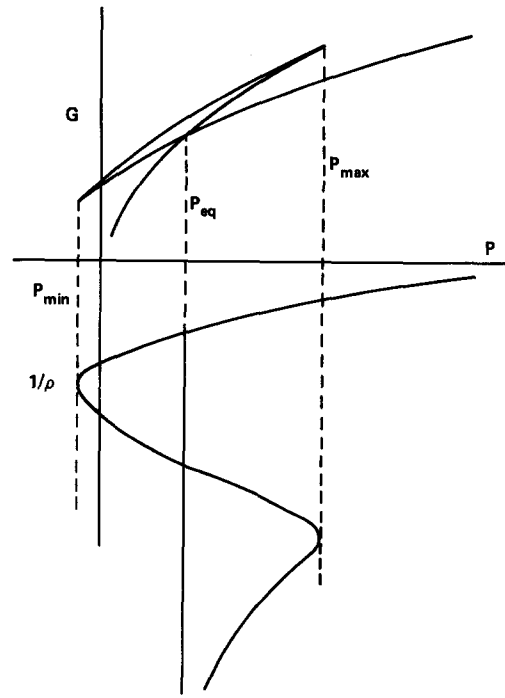
$$p = p_{eq}(T) , \tag{122}$$

FIG. 10. Method for eliminating van der Waals loops in QEOS tables. The equilibrium pressure p_{eq} and the vapor and liquid end point densities are determined by the Gibbs free energy curve.

$$E(\rho,T) = E_l + (E_v - E_l)(1/\rho - 1/\rho_l)/(1/\rho_v - 1/\rho_l) . \tag{123}$$

The Helmholtz free energy and entropy are also interpolated.

VIII. RESULTS FOR VARIOUS MATERIALS

Aluminum is a simple metal, well suited to modeling in the Thomas–Fermi approximation, and it therefore serves as a first test of the results from QEOS. The equation of state of aluminum has been investigated over a very wide range of densities and temperatures.

There have been shock-wave Hugoniot measurements on aluminum to pressures as high as 4000 Mbar; the existing data include laboratory gun experiments and Soviet nuclear-driven shock experiments at the highest pressures.[34] The experimental data and QEOS are compared in Figs. 11(a) and 11(b). The agreement is generally satisfactory.

For the strongest shocks, the shocked state is a completely ionized ideal gas with $\rho/\rho_s = 4$. This limit is approached from above, i.e., greater compressions are achieved for weaker shocks. The physical reason for this is the ionization specific heat which reduces the energy content of the free electrons and thereby reduces the pressure. Near the Hugoniot density maximum ($\simeq 12.5$ g/cm^3), certain other theories predict oscillations in the curve $p(\rho)$ which are attributed to quantum effects of electron shell structure.[34] However, the experiments do not yet have enough resolution to unambiguously detect any such oscillations, and QEOS stands as a satisfactory approximation to the available data.
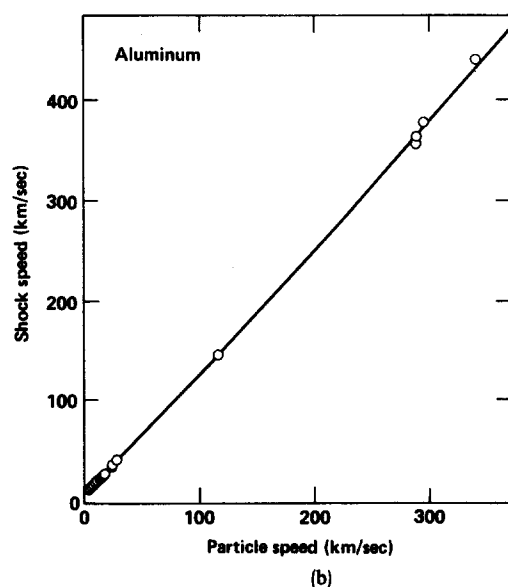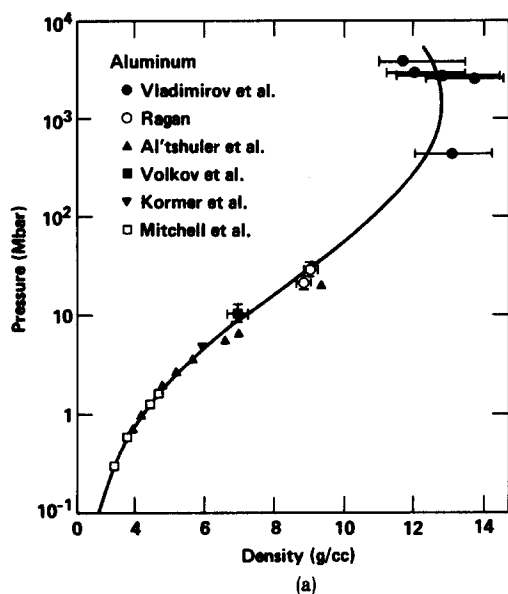
FIG. 11. The aluminum shock Hugoniot. (a) QEOS (solid line) is compared with various high-pressure shock Hugoniot measurements on aluminum. (b) The Hugoniot data of Fig. 11(a) is plotted as particle and shock speeds. QEOS is the solid line.

In Fig. 1 we see that the QEOS adiabats are smooth and well behaved throughout the density-temperature plane.

A separate comparison of the aluminum cold-compression curve was given in Fig. 9; in this case the reference curve is a theoretical quantum-mechanical augmented plane wave (APW) band-structure calculation of high-pressure aluminum and again the agreement is reasonably good.

For the low-temperature (<5 eV) expanded liquid metal, the situation is less satisfactory. Isobaric expansion experiments[35] at ambient pressure $\simeq 1$ kbar give data on aluminum to expansions of a factor 2 (i.e., $\rho = \frac{1}{2}\rho_s$) at $T = 4000$ K. These experiments give equation of state data in a region near the critical point. A soft-sphere van der Waals theory[36] fitted to the isobaric data predicts a critical

point at $T_c = 5726$ K and $P_c = 1.82$ kbar; QEOS gives $T_c = 12\ 140$ K and $p_c = 24.6$ kbar. This error could probably be corrected by generalizing the form assumed for the bonding energy. However, this region is not very important for typical QEOS applications at temperatures above 5–10 eV.

The extensive information available about aluminum enables us to say with some confidence that QEOS is satisfactory for compressions, strong shocks and/or high temperatures (>5–10 eV). It is less satisfactory for the low temperature expanded states.

Experimental Hugoniot data are available for *molybdenum*,[17] a high-density transition metal. These data are compared with QEOS in Fig. 12. The agreement is good. This demonstrates that QEOS can fit transition metals with the same precision as simple nearly free electron metals like Al. In the low pressure expanded states, QEOS fails to give good agreement with experimental data on Mo, as with Al. For example, the soft-sphere theory[36] fitted to isobaric expansion data for Mo predicts a critical point of $T_c = 8000$ K and $p_c = 9.7$ kbar, while QEOS predicts $T_c = 28\ 600$ K and $p_c = 95$ kbar.

Polyethylene is a polymer of CH_2. Each polymer chain is bound by covalent bonding and it interacts with other chains by repulsive closed-shell interactions. QEOS yields a smooth fit to the experimental Hugoniot,[17] as shown in Fig. 13.

Silicon dioxide (SiO_2) is a covalent insulator that shows a series of high-pressure phase transitions to increasingly close-packed crystal structures. The shock Hugoniot[17] shows changes in slope as these transitions are crossed. QEOS does not predict condensed matter (solid–solid) phase transitions, and our best fit is a smooth interpolation between phases, obtained using the pressure multipliers. This is shown in Fig. 14.

Sodium chloride (NaCl) is an ionic solid with a structural transition near 300 kbar. The shock Hugoniot[17] shows this transition as a small deviation from a smooth curve.
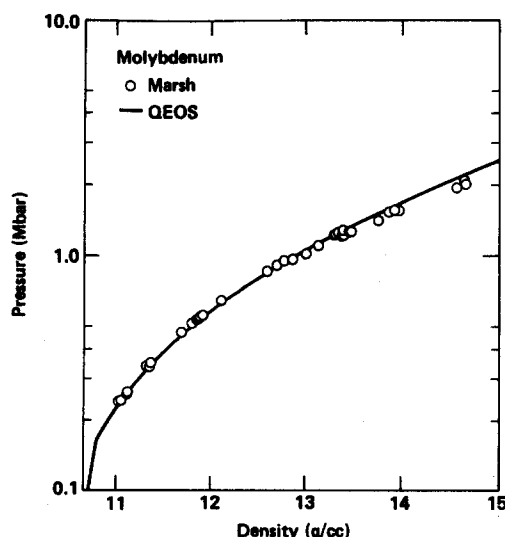

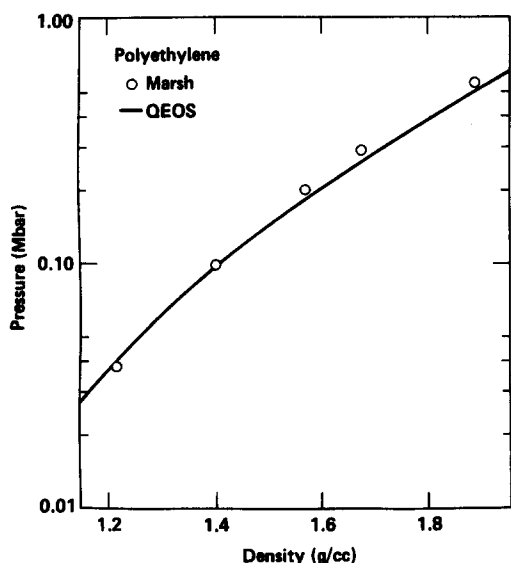FIG. 12. Comparison of QEOS and Hugoniot data for molybdenum.

FIG. 13. Hugoniot comparison for polyethylene, a typical plastic material.

(a)

(b)

FIG. 15. The NaCl shock Hugoniot. (a) The NaCl Hugoniot shows evidence of a phase transition that QEOS does not reproduce. Nevertheless the overall match to the Hugoniot is satisfactory. (b) Shock speed versus particle speed for NaCl.

QEOS produces a good fit to all but the small transition region, as shown in Figs. 15(a) and 15(b).

Hydrogen is a diatomic molecular fluid or solid at 1 bar and is therefore not appropriate for modeling with Thomas–Fermi theory. Nevertheless, the importance of hydrogen in the form of DT to fusion research is so great that an attempt to fit the equation of state with QEOS is worthwhile.

A well-known Livermore EOS table for D_2 is based on experimental isothermal and shock compression data, and upon theoretical models of molecular dissociation and ionization at high temperatures.[37] Various fits and model calculations have been assembled into a complete EOS table by
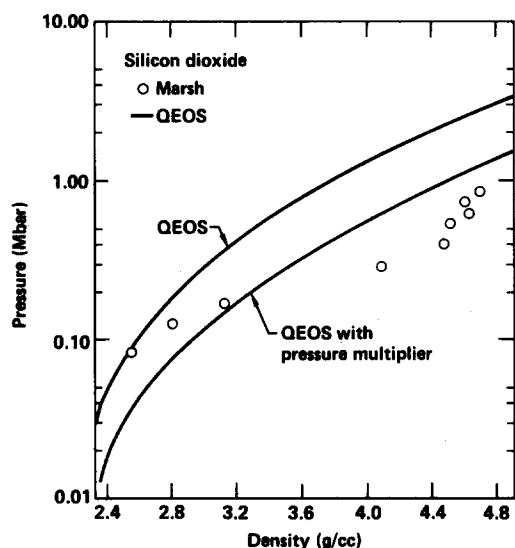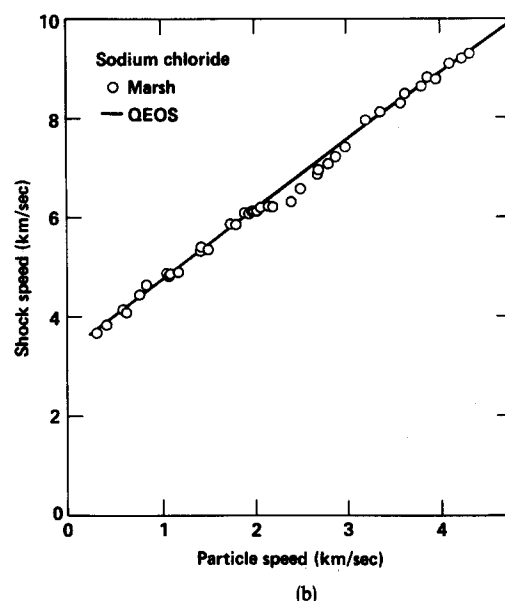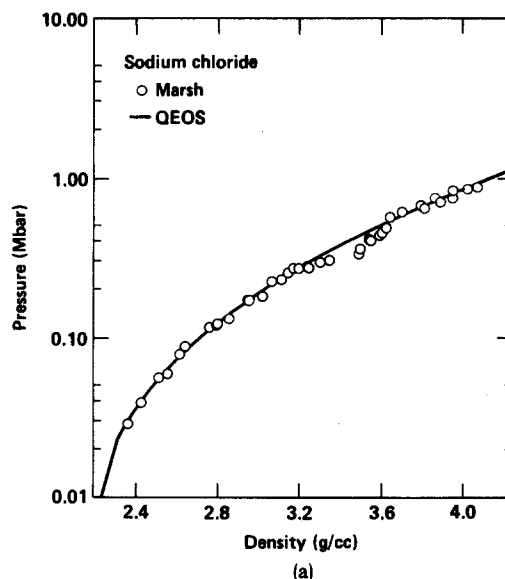

FIG. 14. Example of a poor match to Hugoniot data. Here SiO_2 exhibits a strong phase transition that QEOS is unable to reproduce. With a pressure multiplier the QEOS calculation is closer to the experimental data but still not in agreement. It is unusual to find such a strong phase transition as seen in this case.

interpolating the p and E functions across the gaps between different regions of the (ρ, T) plane. In Fig. 16(a) we compare the Livermore table prediction of the D_2 Hugoniot with that of QEOS, which has been fitted to available experimental shock Hugoniot data[38] and uses a pressure multiplier with $f(0) = 0.5$ to follow the molecular dissociation. The agreement is poor in the 1–10 Mbar region because the tabular EOS predicts a region of high compressibility which results in a very high Hugoniot density. This region is located in an interpolation zone between EOS model regions.

In order to determine which of the two Hugoniots in Fig. 16(a) is more nearly correct, we have performed a series of three theoretical calculations, using independent models.
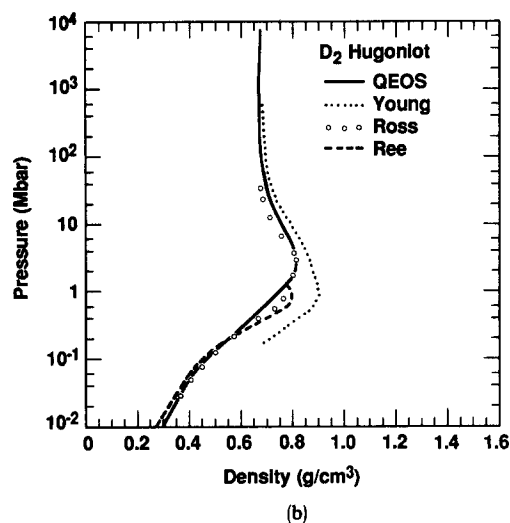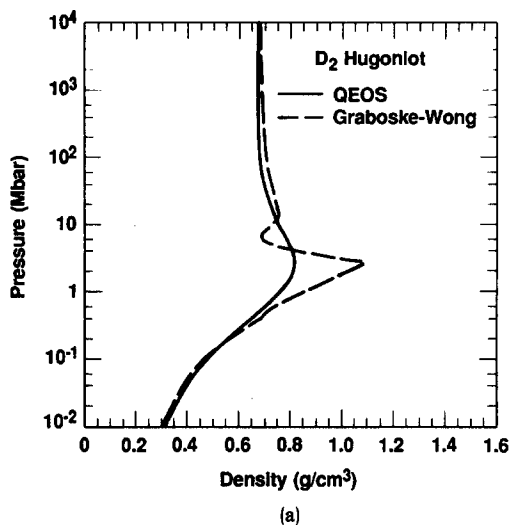
FIG. 16. The deuterium shock Hugoniot. (a) Comparison of shock Hugoniots for D_2: QEOS and a tabular theoretical EOS. (b) Comparison of QEOS and three molecular dissociation models for the D_2 Hugoniot.

These are compared with QEOS in Fig. 16(b). The Young model is a simple ideal gas dissociation–ionization model with a nonideal fluid correction. The Ross model is a fluid perturbation theory with a simple dissociation model added. The Ree model is a fluid perturbation theory of chemical equilibrium which includes the molecular and atomic species. All of these models agree much better with QEOS than with the table, confirming the accuracy of QEOS.

We conclude this section with several general remarks about the expected range of validity of QEOS data. At plasma temperature ($T > 10$ eV) the largest known deficiency of QEOS is its omission of quantum shell effects in ionization. These effects are not large (i.e., approximately 10%) for elements of $Z > 10$ at densities $\rho > 0.01$ g/cm^3; at lower Z or for lower density the shell effects are more important.

At high pressures and low temperatures ($\rho \geqslant \rho_s$, $T < 10$ eV), QEOS obtains rather accurate results because of the way it is normalized to the measured solid density and bulk

modulus. Thus it is often in good agreement with shock-wave data.

Near the normal solid density at temperatures of 2–10 eV, there is a large uncertainty in thermodynamic properties. The dominant physics of this regime is the thermal disruption of chemical bonds in the presence of strong density effects, and QEOS models these phenomena very crudely. In addition, there is little experimental data for this range of conditions and so the uncertainty is especially large.

At densities below the normal solid density for temperatures of 0.01–10 eV, we have critical point data which often disagrees strongly with QEOS predictions. This appears to be the result of unrealistic cohesive energies. However, this has little effect on typical hydrodynamic calculations, and a large error in the critical point location is not necessarily a large error in the equation of state.

IX. COMPUTATIONAL APPLICATION OF EOS DATA

Large hydrodynamic codes such as LASNEX are based on a logic structure that has evolved to become a powerful tool for the solution of problems of pure and applied physics. Because it is natural to extend an existing code to new problems, LASNEX and similar codes have tended to become more flexible, adaptable, and comprehensive.[5] The subroutines that provide physical data have evolved in the same direction.

The following structural elements are found in most large hydrodynamic codes: (a) routines that read a problem statement from an input file, (b) one-time calculations that generate the data and file structures which will be used in this specific calculation, (c) controllers for the series of physics calculations that advance the problem in time, (d) provision for storing or reading a restart file that is a complete record of the status of the calculation, and (e) graphical and text output packages.

The physics calculations naturally divide into two categories: first, algorithms for diffusion, transport, and/or hydrodynamics that couple adjacent zones, and, second, independent calls to one-zone *physics packages* that supply material properties as functions of zonal variables such as density, electron temperature, ion temperature, photon distribution, magnetic or electric fields, etc.

Ideally we can ask that a physics package be designed to have a precisely defined interface with the main code, so that it can be separated, shared with other codes, or replaced. In practice there may be some conflict between this ideal and the need for efficient computation; for example, the input to the EOS routine should logically be a single density–temperature pair but in practice it is significantly faster to input a large array of zonal density–temperature data.

The idealized physics package serves, in effect, as an expert on one branch of physics. It handles any material or mixture of materials. It returns a sensible answer at any density–temperature conditions, and possibly operates also for nonequilibrium (non-LTE) conditions. Suitably organized mathematical and logical tests prevent error conditions that might interrupt the main code calculation. Although high precision is not necessarily required, the physics package should never fail by a large factor. Finally, the package must

3076   Phys. Fluids, Vol. 31, No. 10, October 1988

More *et al.*   3076

be constructed to execute rapidly so that it can be called many thousands of times in a complete simulation. This usually precludes complicated calculations.

The effort to satisfy these objectives represents a new direction typical of modern computational physics and distinct from a more traditional code organization aimed simply at obtaining the most accurate possible answer for one or a few specific cases. Usually a physics package can only hope to achieve the desired generality by placing less emphasis on precision or accuracy. Evidently the physics package, like a good teacher, should select the simplest model that consistently obtains the right answer.

In the light of these general remarks we can survey some points of comparison between QEOS and the usual tabular EOS data libraries. We have found that (1) library tables are often not smooth enough to take numerical derivatives; (2) ion temperature oscillations can result from the need to split an equilibrium table defined for $T_e = T_i$ into separate electron and ion parts for use at $T_e \neq T_i$; (3) strange results are often obtained at or past the edges of the tables; (4) large tables are clumsy in complex calculations involving many materials; (5) there is often a demand for a new table with slightly modified compositions; (6) the new table is usually needed urgently; (7) adiabats found by integrating typical library EOS tables are not a smooth family of curves but often a tangled mess; (8) many library tables are not thermodynamically consistent; and (9) if smoothing or joining techniques have been employed in making a table it is often impossible to determine the source of the specific numbers which appear in the table.

Tabular representation of EOS data has its most severe numerical problems near the two-phase (liquid–vapor) region or near solid density where $\partial p / \partial \rho$ is very large. QEOS employs a tabulated Thomas–Fermi free energy, but avoids these numerical difficulties because the Thomas–Fermi data has only smooth and continuous dependence on density and temperature.

The advantages of tabular representation are the potential higher accuracy of a high-resolution table and a greater lookup speed generally obtained with tabular data. For codes like LASNEX, where EOS lookup is at most a few percent of the calculation, the second reason does not weigh heavily. In our view, QEOS solves the problems (1)–(9) mentioned above with an acceptable overall EOS accuracy.

APPENDIX: EFFICIENT SOLUTION OF SELF-CONSISTENT FIELD EQUATIONS

In this appendix we describe a new algorithm for rapid solution of self-consistent field (SCF) equations derived by a free-energy minimization principle. The method is applied here to the Thomas–Fermi theory but would actually be equally useful for quantum SCF calculations.

We enter the nth cycle of iteration with an *input* electron density $n_i(r)$ subject to

$$\int n_i(r) d^3r = Z. \tag{A1}$$

From this we form a corresponding potential $V_i(r)$,

$$V_i(r) = \frac{Ze}{|\mathbf{r}|} - \int \frac{en_i(r')}{|\mathbf{r} - \mathbf{r}'|} d^3r'. \tag{A2}$$

Then we form an *acting* electron density $n_{a(r)}$ by

$$n_a(r) = c_1(kT)^{3/2} F_{1/2}\{-[\mu_a + eV_i(r)]/kT\}, \tag{A3}$$

where μ_a is adjusted until

$$\int n_a(r) d^3r = Z. \tag{A4}$$

This adjustment of μ_a is done by a subloop using Newton's method and requires the derivative $\partial n_a(r)/\partial \mu_a$. We store the final value of this derivative for later use. Finally we form

$$V_a(r) = \frac{Ze}{|\mathbf{r}|} - \int \frac{en_a(r')}{|\mathbf{r} - \mathbf{r}'|} d^3r'. \tag{A5}$$

If $V_i(r) = V_a(r)$ for all r, the potential is self-consistent and we are finished. If $V_i \neq V_a$, the problem is to select the appropriate mixture of V_i and V_a (or n_i and n_a) as an output which serves as input to the next cycle.

Many workers simply average V_i and V_a (or n_i and n_a). We will instead optimize the choice on the family of functions which are linear combinations of n_i and n_a. After many successful trials we are convinced this approach is sound.

Define

$$\Delta n(r) \equiv n_i(r) - n_a(r), \tag{A6}$$

and let

$$U = e^2 \int \frac{\Delta n(r)\,\Delta n(r')}{|\mathbf{r} - \mathbf{r}'|} d^3r\, d^3r', \tag{A7}$$

$$K = \int \frac{[\Delta n(r)]^2}{\partial n_a(r)/\partial \mu_a} d^3r. \tag{A8}$$

These two quantities are positive whenever Δn does not identically vanish. Here U is evaluated by one-dimensional integrations and is twice the electrostatic self-interaction of a charge density $e\Delta n(r)$. The quantity K is related to the kinetic energy and entropy. Next we form

$$w = U/(K + U). \tag{A9}$$

Obviously $0 < w < 1$. Finally we form the output quantities

$$n_{\text{out}}(r) = n_a(r) + w\Delta n(r), \tag{A10}$$

$$V_{\text{out}}(r) = V_a(r) + w[V_i(r) - V_a(r)]. \tag{A11}$$

This choice of $n_{\text{out}}(r)$ minimizes the free-energy functional $F[n(r)]$ on the one-parameter set of trial functions which

3077   Phys. Fluids, Vol. 31, No. 10, October 1988

More *et al.*   3077

are linear combinations of n_i and n_a, to the accuracy of the second-order expansion

$$F[n(r)] \simeq F[n_a(r)] + w \int \frac{\delta F}{\delta n(r)} \Delta n(r) d^3r$$
$$+ \frac{1}{2} w^2 \int \frac{\delta^2 F}{\delta n(r) \delta n(r')}$$
$$\times \Delta n(r) \, \Delta n(r') d^3r \, d^3r', \qquad (A12)$$

where the derivatives $\delta F/\delta n(r)$ and $\delta^2 F/\delta n(r) \delta n(r')$ are evaluated at $\{n_a(r)\}$.

In fact, these functional derivatives are simply expressed in terms of quantities already available (the proof of this requires careful examination of the preceding equations) as

$$\frac{\delta F}{\delta n(r)} = \mu_a + eV_i(r) - eV_a(r), \qquad (A13)$$

$$\frac{\delta^2 F}{\delta n(r) \delta n(r')} = \frac{\delta(\mathbf{r} - \mathbf{r}')}{\partial n_a(r)/\partial \mu_a} + \frac{e^2}{|\mathbf{r} - \mathbf{r}'|}. \qquad (A14)$$

The explicit form of the Thomas–Fermi functional F is not required further at this point.

The method described has one weakness: when it should converge to a very low electron density, as for the limit of low density and low temperature, the rate of convergence is not very rapid. For this reason we replace Eq. (A10) by a logarithmic-mean formula which reduces to (A10) when $|\Delta n| \ll n_a$ but which moves more rapidly toward zero in the regions where $n_a(r) = 0$.

With this modification we have a very successful procedure that typically takes only a few (4–8) cycles to achieve convergence. Because Eq. (A9) is producing a single number (w), it appears that it could also be used for quantum self-consistent field calculations even with the Thomas–Fermi approximation to the kinetic energy density in Eq. (A8).

[1]See Physics of High Energy Density, edited by P. Caldirola and H. Knoepfel, Proceedings of the International School of Physics "Enrico Fermi," course 48 (Academic, New York, 1971).

[2]R. P. Feynman, N. Metropolis, and E. Teller, Phys. Rev. 75, 1561 (1949).

[3]J. F. Barnes, Phys. Rev. 153, 269 (1967).

[4]The Cowan theory is partially described in National Technical Information Service Document No. LA-7313-MS (Los Alamos National Laboratory report LA-7313-MS, by C. W. Cranfill and R. M. More, 1978). Copies may be ordered from the National Technical Information Service, Springfield, Virginia 22161. The price is $9.95 plus a $3.00 handling fee. All orders must be prepaid.

[5]See National Technical Information Service Document No. DE84017287 (Laser Program Annual Report for 1983, LLNL Report No. UCRL-50021-83, by R. M. More and G. B. Zimmerman, pp. 3–55). Copies may be ordered from the National Technical Information Service, Springfield, Virginia 22161. The price is $36.95 plus a $3.00 handling fee. All orders must be prepaid.

[6]R. M. More, J. F. Barnes, and R. D. Cowan, Bull. Am. Phys. Soc. II 21, 1153 (1976).

[7]Y. T. Lee and R. M. More, Phys. Fluids 27, 1273 (1984).

[8]R. M. More, in Laser–Plasma Interactions 3, edited by M. B. Hooper, Proceedings of the 29th Scottish Universities Summer School in Physics (Camelot, Southhampton, 1986), p. 157.

[9]B. Ya. Zel'dovich and Yu. P. Raizer, in Physics of Shock Waves and High-Temperature Hydrodynamic Phenomena (Academic, New York, 1966), Chap. 1.

[10]M. Ross, Rep. Prog. Phys. 48, 1 (1985).

[11]S. G. Brush, Prog. High Temp. Phys. Chem. 1, 1 (1966).

[12]D. A. Kirzhnitz, Yu. Lozovik, and G. V. Shpatakovskaya, Usp. Fiz. Nauk 117, 3 (1975) [Sov. Phys. Usp. 18, 649 (1976)].

[13]See AIP document no. PAPS PFLDA-31-3059-245 for 245 pages of Lawrence Livermore National Laboratory report "Atomic Physics in Inertial Confinement Fusion" [Report No. UCRL-84991 (1981) by R. M. More]. Order by PAPS number and journal reference from American Institute of Physics, Physics Auxiliary Publication Service, 335 East 45th Street, New York, NY 10017. The price is $1.50 for each microfiche (98 pages) or $5.00 for photocopies of up to 30 pages, and $0.15 for each additional page over 30 pages. Airmail additional. Make checks payable to the American Institute of Physics.

[14]V. A. Alekseev, V. E. Fortov, and I. T. Yakubov, Usp. Fiz. Nauk 139, 193 (1983) [Sov. Phys. Usp. 26, 99 (1983)].

[15]A. V. Bushman and V. E. Fortov, Usp. Fiz. Nauk 140, 177 (1983) [Sov. Phys. Usp. 26, 465 (1983)].

[16]B. K. Godwal, S. K. Sikka, and R. Chidambaram, Phys. Rep. 102, 121 (1983).

[17]LASL Shock Hugoniot Data, edited by S. P. Marsh (University of California Press, Berkeley, 1980).

[18]See National Technical Information Service Document No. DE85011902 (Los Alamos National Laboratory report LA-10160-MS, by K. Holian, 1984). Copies may be ordered from the National Technical Information Service, Springfield, Virginia 22161. The price is $30.95 plus a $3.00 handling fee. All orders must be prepaid.

[19]R. M. More, in Atomic and Molecular Physics of Controlled Thermonuclear Fusion, edited by C. J. Joachain and D. E. Post (Plenum, New York, 1983), p. 399.

[20]D. B. Boercker and R. M. More, Phys. Rev. A 33, 1859 (1986).

[21]R. M. More, in Atoms in Unusual Situations, edited by J. P. Briand (Plenum, New York, 1987), p. 155.

[22]E. Fermi, Thermodynamics (Dover, New York, 1956).

[23]R. Grover, J. Chem. Phys. 55, 3435 (1971).

[24]M. Baus and J.-P. Hansen, Phys. Rep. 59, 1 (1980).

[25]W. G. Hoover, G. Stell, E. Goldmark, and G. Degani, J. Chem. Phys. 63, 5434 (1975).

[26]N. F. Mott and H. Jones, Theory of the Properties of Metals and Alloys (Dover, New York, 1958).

[27]J. Matthews and R. L. Walker, Mathematical Methods of Physics (Benjamin, Reading, MA, 1970), 2nd ed., Sect. 2.2.

[28]J.-P. Hansen and I. R. McDonald, Theory of Simple Liquids (Academic, New York, 1976).

[29]K. A. Gschneidner, Jr., Solid State Phys. 16, 275 (1964).

[30]R. M. More, Adv. At. Mol. Phys. 21, 305 (1985).

[31]J. Scott, Philos. Mag. 43, 859 (1952); J. Schwinger, Phys. Rev. A 22, 1827 (1980).

[32]R. M. More, Phys. Rev. A 19, 1234 (1979).

[33]A. K. McMahan and M. Ross, in High Pressure Science and Technology, edited by K. D. Timmerhaus and M. S. Barber (Plenum, New York, 1979), Vol. 2, p. 920.

[34]D. A. Young, J. K. Wolford, F. J. Rogers, and K. S. Holian, Phys. Lett. A 108, 157 (1985).

[35]G. R. Gathers and M. Ross, J. Non-Cryst. Solids 61 & 62, 59 (1984).

[36]See National Technical Information Service Document No. UCRL-52352 (LLNL Report UCRL-52352, by D. A. Young, 1977). Copies may be ordered from the National Technical Information Service, Springfield, Virginia 22161. The price is $9.95 plus a $3.00 handling fee. All orders must be prepaid.

[37]H. C. Graboske, Jr. and K. L. Wong (private communication).

[38]W. J. Nellis, M. Ross, A. C. Mitchell, M. van Thiel, D. A. Young, F. H. Ree, and R. J. Trainor, Phys. Rev. A 27, 608 (1983).